Encapsulated Source Contact Dose Estimates incorporating Secondary Electron Emission

by

James Cleary, B.Eng.

Under the supervision of Dr. Edward Waller

A thesis submitted in partial fulfillment of the requirements for the degree of

Master of Applied Science in Nuclear Engineering

In the Faculty of Energy Systems and Nuclear Science graduate program

University of Ontario Institute of Technology

April, 2015

ABSTRACT

Secondary electron emission generated at the surface of thin material from interaction with gamma rays form a significant component of the surface dose. The intensity of this emission is known to vary with material composition and incident radiation energies. The goal of this research effort is to estimate the emission strength from radioactive sources utilized in the early history of cancer Brachytherapy, and develop dose conversion factors from that data. Data was obtained by utilizing a comparative stochastic analysis, conducted with the Monte Carlo radiation transport code MCNPX. Emission intensities were measured at the surface of source encapsulation and at increasing distances in tissue equivalent material. It is shown that the results obtained correlate to the historical trends, however the electron component of the simulated emission is of greater by several orders of magnitude than that previously estimated. The dose conversion factors found from simulation will assign a higher absorbed dose than those currently published. The corollary is that the current published values are under attributing dose for a given radiation injury, which hinders effective treatment.

ACKNOWLEDGEMENTS

I would like to express my profound gratitude toward my academic and research supervisor Dr. Ed Waller for his expert guidance and generous encouragement throughout the completion of this work. In addition I would like to thank Dr. Franco Gaspari for serving as my external examiner, and Dr. Anthony Waker from the Faculty of Energy Systems and Nuclear Science.

I am deeply beholden to the Natural Sciences and Engineering Research Council of Canada (NSERC) Industrial Research Chair Program for funding the duration of this research.

My thanks to all of the people I have known at the University Of Ontario Institute Of Technology who have enriched my time there and elevated my understanding.

I especially need to thank my longsuffering wife, without whom I would not be where I am today, for her love, affection and uplifting nature over the time we have been together. A final thanks to my family who have been there for me since the outset of my studies and have blessed me with their support and objective thoughts when I needed them the most.

Contents

LIST OF FIGURES

LIST OF TABLES

Chapter 1 INTRODUCTION

Radiation, in all of its forms, is known to interact with material by liberating the atomic electrons bound in the rest state orbitals. The interaction may be direct where a collision imparts the required energy, or indirectly where if the incident radiation is charged the attractive or repulsive forces will also impart the required energy, where the net result is the ionization of the atom. An ionized atom is inherently unstable and naturally seeks to return to a low potential configuration by neutralizing the net charge. This is accomplished by adding an electron from another source, where the electrons being added are not likely free but bonded to another atom, where the bond is weaker than the attractive force of the ion. The result is the production of additional ions in material proximal to the ionized atom, which induces propagating damage. Of greatest concern is this type of cascading action in living tissue where DNA and other critical components of living cells may be damaged resulting in cell apoptosis and chromosomal aberration from faulty repair.

The amount and of ionization is dependent on the type of radiation (i.e. if it is a charged particle), and the energy of the emission. Generally, a higher amount of damage is incurred in tissue for a radioactive insult involving charged particles. This type of hazard must be identified and quantified where present, to ensure that accurate radiation protection practices may be applied.

One area of interest is the radiation field seen at the surface of an encapsulated gamma ray source. The contact dose rate at the surface there incorporates elements of primary gamma and secondary electron radiation from gamma ray interactions in the capsule wall. Secondary electrons are known to cause direct and indirect ionization of material which is observed as biological damage in living tissue. Therefore, the

secondary electron component is a major factor of the absorbed dose for a contact exposure. Precise surface dose rate values contribute to effective implementation of: radiation implant therapy, industrial protection standards, and forensic dose analysis.

Historically, this hazard has been explored by experiments carried out during the early development of radium therapy for interstitial application. The available technology of the period made exact quantification impossible, and most experiments stated a relative intensity of the secondary electron emission relative to the total emission, but not an exact proportion of the condition at the surface. Exact values are published in the National Council for Radiation Protection & Measurements, Report Number 40 (NCRP-40) which provides the surface dose rate for encapsulated sources of Ra-226, Ir-192, Cs-137 and Co-60, and the required correction factors to account for secondary electron contribution. These factors are used in the present era to assign dose retrospective absorbed dose values for a contact exposure to an encapsulated gamma source.

1.1 Background and Motivation

Treatment of personnel that have incurred localized radiation injury from encapsulated sources is based on the committed dose which is calculated using dose conversion factors such as those published in NCRP Report No. 40. The lack of precise factors will result in a misattribution of the dose and potentially insufficient treatment leading to necrosis and infection of tissue.

The basis of the correction factor for secondary electron emission and the resultant dose conversion factors originate from the body of work performed historically in the study of radium brachytherapy[1]. It is known that those experimental trials measured emission for encapsulated sources somewhere near the surface and then extrapolated measured values to the surface region to obtain dose rate data for the surface condition. This method was required as the design of the detectors of the time did not allow examination at the region very near the source surface, where it is suspected that secondary electron emission dominates the dose rate. The rationale for an updated study, using a numerical simulation, is substantiated based on the increase in the precision of measurement available at the present time. Additional evidence supporting an updated study has been seen in medical cases where the observed symptomology does not align with the assigned dose based on the conversion factors described above.

[1] These cases are discussed in Section 2.3 and 2.4 of the thesis

1.2 Overview of Secondary Electron Emission

The central focus of this work is an examination of the surface dose rate from and encapsulated gamma ray source, and the contribution to that from secondary electrons. The mechanism by which this effect occurs must be understood in order to make appropriate conclusions which will guide the resulting proposed radiation protection practices.

In the source configuration studied in this thesis, secondary electrons are predominantly produced by two phenomena: the Photoelectric Effect and Compton Scattering, which are described below.

The Photoelectric Effect for a given material is expressed as a function atomic number and incident energy for the gamma ray. The cross section is proportionally dependent on the Z number of the material, and increases exponentially with the energy of the incident photon, as in Eqn 1 (Baratta & Lamarsh, 2001):

$$\sigma_{pe} = Z^{n(E)} \qquad \textbf{Eqn(1)}$$

Where 'n' is a variable that is a function of energy.

For Compton scattering, the secondary electron production cross section, σ_C, is expressed as a function of the atomic number of the incident material, and the rest mass energy cross section of an orbital electron, ${}_e\sigma_C$, (Eqn 2) (Baratta & Lamarsh, 2001):

$$\sigma_C = Z \times ({}_e\sigma_C) \qquad \textbf{Eqn(2)}$$

Thus, as the atomic number of material within which the interaction is occurring increases, the proportion from the Compton scatter will decrease in proportion to the total while the contribution from the Photoelectric Effect will increase, which can be seen in Figure 1:

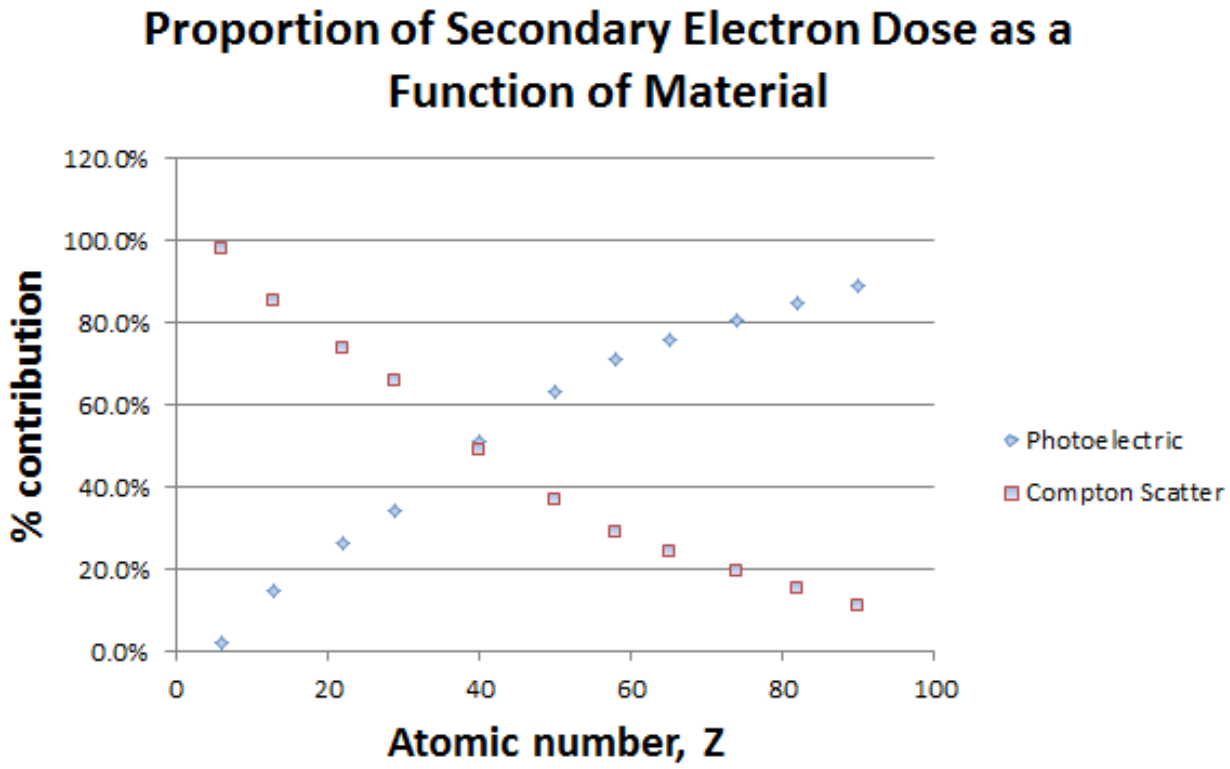

Figure 1 : Percent contribution of Photoelectric and Compton electrons to the total secondary elecrton emssion as a function of atomic number

The increase in secondary electrons is not a linear increase since the production is also a function of material density. This dependence is shown in the following Eqn 3 to Eqn6:

For short wavelength radiation incident on a thin sheet of material the value of the secondary electron emission is given Eqn(3) as stated by Wilson (1941):

$$W = (\sigma_{pe} + \sigma_C) I_0 \frac{2}{3} r \qquad \textbf{Eqn(3)}$$

Where

- W is the amount of secondary electrons generated
- I_0 is the intensity of the incident radiation,
- σ_{pe} is the photo-electric absorption coefficient
- σ_C is the true absorption coefficient associated with scattering.
- r is the thickness of the material of the wall

As all cases explored in this thesis examine secondary electron emission for changing shielding material of equivalent thicknesses. The wall thickness can then be said to be inversely proportional to density. Therefore Eqn(3) may be restated as a proportion:

$$W \propto \left(\frac{\sigma_{pe}}{\rho} + \frac{\sigma_C}{\rho}\right) \qquad \textbf{Eqn(4)}$$

Where

- ρ is the density of the capsule material

However, the production of secondary radiation is proportional to the orbital electron density which is equivalent to the atomic number of the material, and thus Eqn(4) may be rearranged to show the density variable in terms of electron density and atomic weight:

$$W \propto (\sigma_{pe} + \sigma_C) \times \frac{NZ}{A} \qquad \textbf{Eqn(5)}$$

Where

- N is Avogadro's number
- Z is the atomic number
- A is the atomic weight

For a single atom we may remove 'N':

$$W \propto (\sigma_{pe} + \sigma_C) \times \frac{Z}{A} \qquad \textbf{Eqn(6)}$$

Therefore, with an increase in atomic number, the increase in the first term is smaller for the lower atomic numbers than the decrease in the second term, such that there is a net decrease in the production of secondary electrons to a minimum. Beyond this, the trend reverses and the increase in the first terms surpasses the continuing decrease in the second term (Wilson, 1941). The increase is due to the change in contribution from the Photoelectric Effect cross section with increasing atomic number, where the decrease is due to attentional attenuation and in the encapsulation material. This behaviour is shown in Figure 2 in Section 2.2.

The relationship shown above illustrates the importance of correct material selection for source capsules to reduce (or maximize) the secondary electron emission in an encapsulated source system. Historically,

the capsule is designed to shield any source beta emission, which is unwanted in most applications, and to contain the source in a deliverable format. However this encapsulation results in the production of secondary electrons. This secondary field requires the application of an additional filter/shield to minimize the relative dose contribution. The material design of the second filter must be selected so that the additional interaction of gamma rays there will not create an objectionable amount of secondary electron radiation.

1.3 Research Goals and Approach

The purpose of this work is to perform numerical simulations using stochastic simulation software to model radioactive emission at the surface of an encapsulated source, as a function of encapsulation material will also be studied. The data obtained from this simulation will provide a dose conversion factor for the source type modelled. The dose conversion factor is based on the gamma radiation present at the surface and secondary electrons that are produced from the source gamma interaction in the capsule walls. This secondary electron radiation is known to be of lower energy and thus the range is limited to approximately 1 mm depth in tissue. This study evaluated the tissue region from source surface to 1 mm depth using simulated source models developed from those used in the physical experiments for radium therapy studies[2]. The simulation data is evaluated against those physical trials and new dose conversion factors are proposed based on the differences.

[2] These studies are discussed in Section 2.2 and 2.3 of this thesis

1.4 Thesis Outline

This thesis consists of five chapters, where Chapter 1 outlines the required background, motivation and objectives of this study. Chapter 2 provides information related to the previous research completed which the current study references to reproduce experimental data based on those methods. Included is a review of current dose conversion factors for encapsulated sources and the studies that are used to support the values. The numerical modelling method used to simulate the transport and energy deposition from interaction of secondary electrons is described in Chapter 3 along with a description of the model design and specifications. The simulation is completed in two parts: first, verification of trials cited supporting the dose rates stated in NCRP-40, and second simulations to produce revised dose conversions factors comparable to those published in NCRP-40. Chapter 4 presents the results of the simulation data, and the results are described for significance and compared to the historical studies which provided the framework for the simulation. The significance of any observed deviation is highlighted there. Chapter 5 summarizes the findings of this thesis providing the concluding analysis and recommendation for future work .

Chapter 2 LITERATURE REVIEW

The references examined as a part of this thesis originate from trials performed in the early 20th century radium therapy studies, related to brachytherapy. This data was used to construct dose conversion factors for select encapsulated gamma sources, which were published in 1972 by the National Council for Radiation Protection and Measurements, and is currently used as a reference to attribute dose from contact exposures. This section describes the NCRP-40 data and the associated reference documents which were used in the compilation.

The focus of this chapter is an examination the experimental results and methods used in the historical studies, assessing the accuracy of those studies, which will provide a basis for developing a model to verify selected works with a numerical simulation. This model will be executed to determine the secondary electron emission at the source surface as a function of encapsulation material, and the relative intensity of the secondary electron emission to the gamma emission at the source surface. This data may then be used to determine dose conversion factors for the surface dose rate applicable to an encapsulated gamma source, which can then be compared to biological markers[3] seen in living tissue for accidental exposures. Dose conversion factors are commonly used to ascribe absorbed dose for an exposure scenario where the surface dose rate is not easily determined.

[3] Biological marker commonly referred to in the literature reviewed in this thesis is erythema

2.1 Medical Treatment Basis to Dosimetry

The dose conversion factors which this thesis reproduces using a numerical simulation, were originally published in the National Council on Radiation Protection and Measurements, Report No. 40 (NCRP, 1972) for contact dose rates of various encapsulated gamma emitting sources. The report describes surface dose rates for typical encapsulated sources (needles) used in medical interstitial treatments, where the dose rates for photon emission are listed with an additional correction factor recommended to account for the dose contribution from secondary electron radiation (Table 1). The correction factors were not calculated, but empirically estimated from published values obtained in physical trials examining encapsulated radium sources. Since the supporting data was limited to radium, the additional radionuclides listed have correction factors that were obtained using theoretical enhancement factors, based on the radium studies.

Table 1: Approximate Gamma Ray Dose to the Hand for 1 Curie in a sealed source (adaptation of Table 6 from NCRP-40 (1972))

Radionuclide	Surface Dose Rate (R/min-Ci)	Surface Dose Rate Corrected for Secondary Electron Production (R/min-Ci)
Cs-137	513	513 + 45%
Co-60	2075	2075 + 45%
Ir-192	813	813 + 45%
Ra-226	1310	1900

The significance of the dose conversion factors recommended by NCRP-40 is seen in cases of retrospective dose attribution where dose is assigned for an exposure to an encapsulated gamma source based on those factors (Saenger, Kereiakes, Wald, & Thoma, 1974).

To gain an understanding of the origin of the conversion factors recommended in NCRP-40, the reference documentation cited in that report was also examined. The reference cited is the report titled “Dosimetry in Implant Therapy” (Shalek, Stoval, Attix, & Tochilin, 1969). The data from this document is the basis of the dose conversion factors published in NCRP-40, and is detailed below in Section 2.2.

2.2 Secondary Electron Studies

The publication "Dosimetry in Implant Therapy" (Shalek, Stoval, Attix, & Tochilin, 1969) is the primary reference for the dose conversion factors for encapsulated sources published in NCRP-40 (NCRP, 1972). The chapter on brachytherapy entitled "Secondary Electron Generated in the Capsule Wall" pp748 (Shalek, Stoval, Attix, & Tochilin, 1969) describes the relative intensity of emission for encapsulated Ra-226 source as a function of encapsulation material. This section describes the phenomena of secondary electron radiation and the dependence of forward scattering of electrons on the atomic number of the capsule material. The data published in that report was not original research, rather was a compilation from studies conducted by Benner (Benner, 1931), Quimby (Quimby, Marinelli, & Blady, 1939), and Piccard and Stahel (1930), see Figure 2.

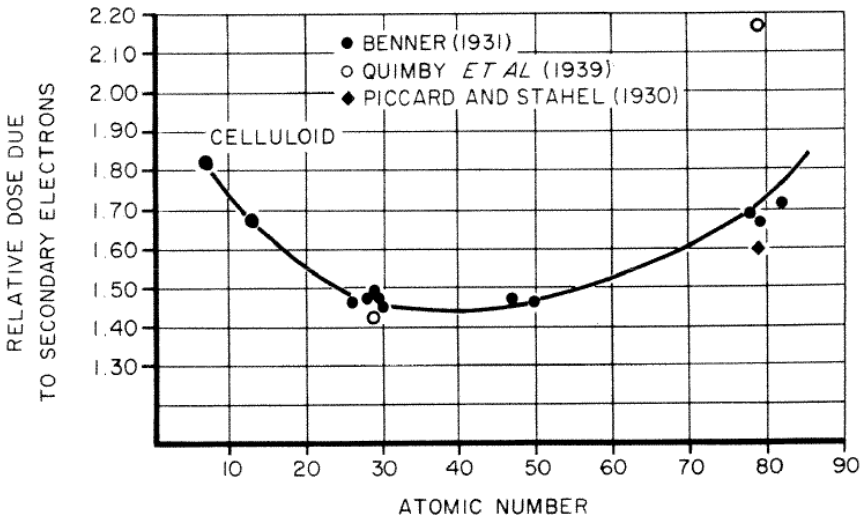

Figure 2: Relative surface dose from secondary electrons as a function of atomic number of capsule material (Shalek, Stoval, Attix, & Tochilin, 1969)

Figure 2 shows the ratio (relative contribution) of total emission to the gamma only emission at the surface of the source for encapsulations of increasing atomic number, per the following ratio:

$$\frac{Total\ Dose\ Rate}{Gamma\ only\ Dose\ Rate}$$

Data from this trend was used in NCRP-40 to obtain the recommended enhancement factors for contribution of secondary electron emission to the surface dose rate of an encapsulated radium source.

To assess the precision of the data referenced in Figure 2, the applicable publications were reviewed and are described in the next section (Benner, 1931), (Quimby 1939).

2.3 Experimental Investigation of Secondary Electron Phenomena

One of the studies referenced by Attix (1969) is that conducted by Benner (1931) designed to assess the intensity of the total radioactive emission and the component from secondary electron radiation for encapsulated radium sources, as a function of capsule material. The emission intensities vary with the material change based on the shifting dominance of the source of secondary electron generation, from Compton scattering to the Photoelectric Effect with an increase in the Z value as described in Section 1.2.

Benner (1931) explores the phenomena, and performs experiments where the intensity is measured for the total emission and the for the photon component only. Encapsulation materials are used from atomic number 6 to 82, at intervals of approximately 10. Results are tallied in units of current, which are proportional to the intensity of the beam. Taking the difference of the total and the photon only

intensity values, and dividing by the photon only, gives a ratio that is commonly referred to as the secondary electron correction factor, which is described as follows:

$$\frac{(Total\ Dose\ Rate)-(Primary\ Gamma\ Dose\ Rate)}{(Primary\ Gamma\ Dose\ Rate)}$$

NCRP-40 lists correction factors in the form shown above for encapsulated sources based on this physical experiment. These factors are also seen in the experiments conducted by Benner (1931) where the minimum electron correction factor is a 40-50% increase in the photon only hazard for mid-range atomic number encapsulations, and nearly 90% increase for the highest and lowest atomic numbers (Figure 2).

However, the Benner study did not include a conversion of the result to a dose rate, as the focus of that work was to determine the relative proportion of the emission from secondary electron. Thus, the author notes that the trend determined is valid, but requires a correction term to obtain real values dose, which was not completed as a part of that study. The detection apparatus consists of an air ionization chamber located near the source composed of an iron shell and a brass collecting electrode, where the emission enters through a thin aluminum window. When radiation enters the chamber it directly and indirectly induced ionizations in the gas which is translated into a measurable current via collecting electrodes. A consequence of this this setup are two dominant error sources, first is secondary electrons are produced via photon interactions with the chamber material which are detected in addition to the source emission, and second not all secondary electrons generated at the source are detected as the source is located away from the detector in air, and the entrance to the detector is a thin window of solid material. The detection chamber and the source are separated by a distance of about 2 centimeters, which precludes a quantification of the total emission spectrum as some components would be of lower energy and would

not be able to reach the detector. Additionally the aluminum window adds a factor of attenuation which further eliminates some emission from detection.

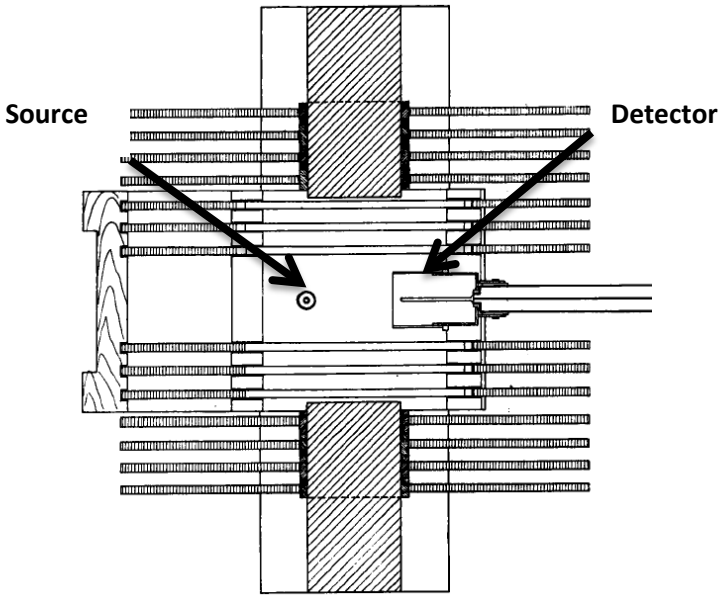

Figure 3: Apparatus (source and detector) used by Benner (1931)

A consequence from these factors is that the surface dose was not completely recorded, with the majority of the omission applicable to the secondary electrons, therefore the results obtained from this experiment are not precise for use in describing the hazard at the source surface. NCRP-40 does however apply this data to quantify the secondary electron emission from encapsulated sources.

This experiment could be retried in the present day with a physical apparatus, where improvements can be made on this detector design. These should include a current measuring device that is sensitive enough so that electron emission in a vacuum chamber could be detected without the need for additional ionizations in a gas type detector. If a gas type detector must still be used, appropriate calibration factors and efficiency correction should be applied to ensure that the dose rate measured is accurately assessed for surface conditions.

Despite the misalignment in referenced data, the work by Benner (1931) is valuable as the intensity of the secondary electron emission is quantified separately from the accompanying gamma dose. This information provides an indication of the magnitude of the dose components near the source surface, which are required to obtain a secondary electron correction factor and dose conversion factor as described in Section 2.2. This type of data is required from the simulation to develop the secondary electron correction factors and dose conversion factor for the total emission.

2.4 Extension to other Encapsulation Materials

The study by Quimby (1939) which is also referenced by Attix (1969), investigates the aforementioned phenomena of changing secondary electron emission intensity as a function of encapsulation material (Figure 4).

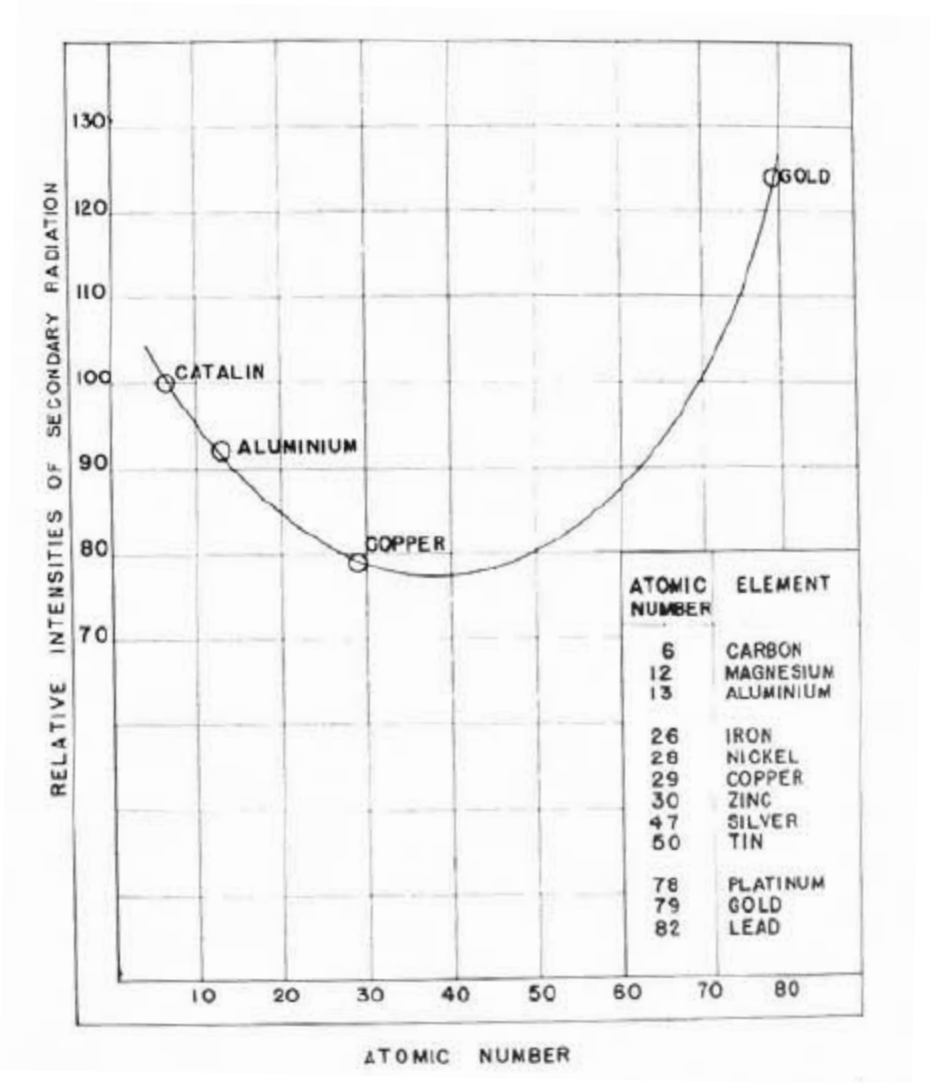

Figure 4: Intensities of secondary electron emission (percent), as a function of atomic number of encapsulation. All data point values relative to data point "CATLIN"

Similar to the data from Benner, the Quimby data forms part of the trend stated by Attix (1969), referenced in NCRP Report No. 40, to describe the correction factors for encapsulated Ra-226 sources (NCRP, Protection Against Radiation from Brachytherapy Sources, 1972). The parameter measured by Quimby (1939) is the intensity of the total beam in units of ionization/current as detected for emission from Ra-226 sources, which were encased in varying materials of equal shielding thickness. In contrast to Benner, Quimby (1939) does not separate the beam and only makes a comparison of the data relative to the first measured data point (Figure 4). Thus, the data can only be referenced as a trend, since the discrete quantity of the secondary emission is not known. The trend is then fitted to the absolute data measured by Benner and that shown in the summary by Attix see Figure 2.

An additional difference in the Quimby study with respect to Benner is the location of the detector. Benner located the detector some distance from the source, while in Quimby the source capsule forms a part of the collecting electrode, and the detector is concentric with the source. Quimby measures the emission at decreasing distances approaching the source surface, where the space between the ionized volume and the radium capsule are reduced, and a final value for a zero distance (surface) is obtained from extrapolation. This difference enables the determination of a result that more closely resembles the conditions at the source surface. This may be observed by comparing the trend line in Figure 4 Quimby, with Figure 2 Attix.

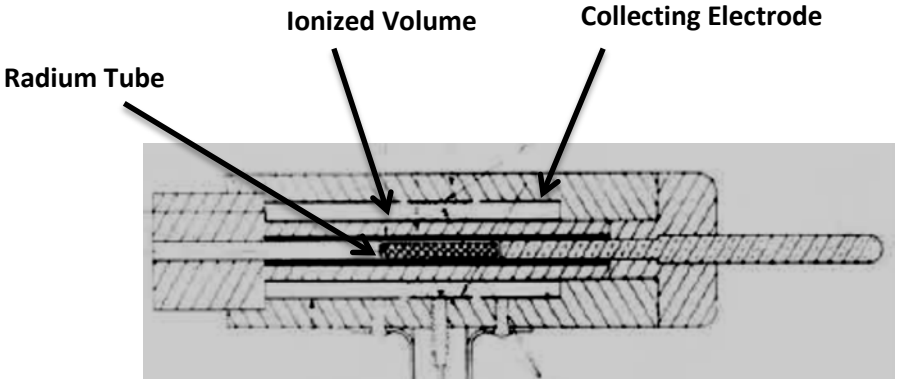

Figure 5: Diagram of Ionization Chamber (Quimby, 1939)

From this comparison, it is determined that the Benner experiments describe the surface emission from an encapsulated gamma source less accurately than those performed by Quimby, based on the detector designs. Additionally, the deviations shown in the Quimby data was not taken into account in the formation of the correction factors stated in NCRP-40, or the compilation stated by Attix in Figure 2. The Quimby (1939) study alone however cannot provide the required secondary electron correction factors, as the individual secondary electron intensities are unknown in those experiments.

The Quimby study also performed trials to substantiate the measured emission intensity. The tissue of living human subjects was exposed to the Ra-226 source for varying encapsulations of equivalent shielding thickness as described above. The intensity of the resultant erythema was photographed and described. For equal duration exposures the magnitude of the erythema shows differences in good agreement with the measured values as the material of the encapsulation changes from catalin to gold Figure 6. The most severe reactions provoked were seen for the encapsulations of highest atomic number (gold), which corresponds to the highest measured emission.

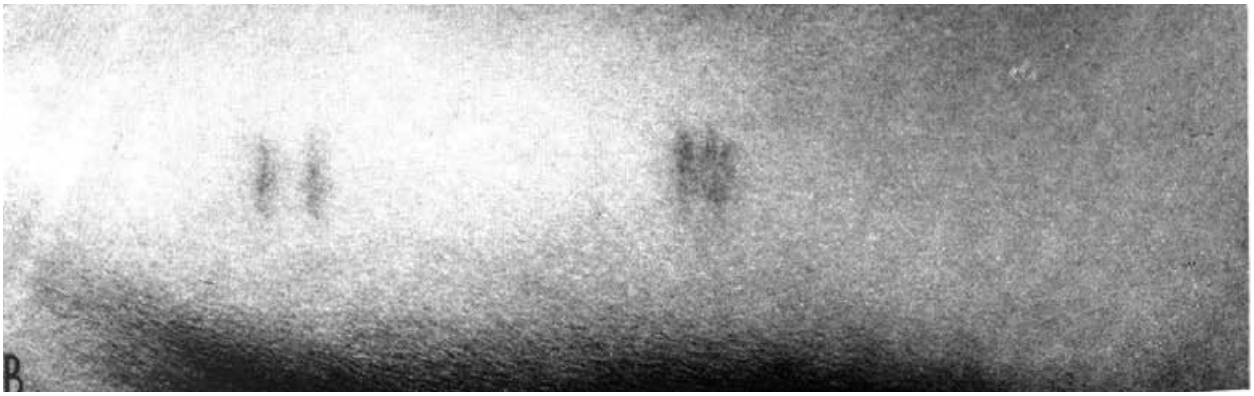

Figure 6: Erythema from exposure of living human tissue to encapsulated sources, upper arm (Quimby, 1939)

A final component of the Quimby (1939) study examines the range of the secondary electrons produced by Radium-226 sources for varying encapsulations. This data from this component is used in this study to verify the numerical simulation, and is described in Section 3.2.

2.5 Additional Investigations Reviewed

An additional study was reviewed to demonstrate the application of the dose conversion factor stated in NCRP 40 in cases of accidental radiation injury requiring forensic dose attribution (Saenger, Kereiakes, Wald, & Thoma, 1974). A final study has also been included by Tripathi (1977), to illustrate the results of a study of the emission from encapsulated sources which is not directly referenced by NCRP-40 or those studies connected with that report.

2.5.1 Tc-99m Depth-Dose

The study by Tripathi (1977) performs a simulated depth dose assessment for encapsulated Tc-99m sources using a Monte Carlo simulation. The exact technique is not well described, however it is based on a software Monte Carlo code developed by the author. This study is reviewed as a part of this thesis to demonstrate that other authors have also examined the surface emission from encapsulated gamma sources separate from work connected to NCRP-40. This additional study serves as a means of comparison to the studies reviewed in the previous section of this thesis.

In this study, the depth dose rate in living human tissue was determined for the emission from an encapsulated source of a radiopharmaceutical preparation of Tc-99m, which is equivalent to a low energy gamma source encapsulated in a polymer (low Z number) material. The health hazard associated with material handling of these sources is the motivation of the study, with a focus on external exposure. All results in that study relate to an external case where dose is recorded only at the active region of skin at depth 0.02 - 0.1 cm, where deposition in the epidermal tissue layer is discounted, as the tissue is nonliving.

The Tripathi study identifies a gap in a typical method dose assignment, where calibration curves used to assess the dose received by the technicians are based on thermoluminescent dosimeters (TLD), which are applicable for gamma ray and high energy beta, but do not adequately measure the increased hazard at source surface from secondary electron radiation, as the range is insufficient to reach the detector. The result is an underestimation of the dose deposition at distance near the source from 0-1 cm. This incomplete dose assignment is in concert with the motivation of the current study, where the NCRP-40 references are hypothesized to have measured incomplete values of the surface emission intensity.

The results from Tripathi, show a very high surface dose rate followed by a sharp drop off with increasing distance in tissue away from the source (Figure 7). This trend is consistent with the results seen in similar studies examining dose depth relation (Quimby, Marinelli, & Blady, 1939), where the intensity of the emission increased with decreasing distance to the source. The sharper drop in the Tripathi data is likely due to the lower energy gamma ray emission of the Tc-99m relative to Ra-226, which would produce a soft spectrum secondary electron emission that would be seen predominantly at the very near distances to the source surface.

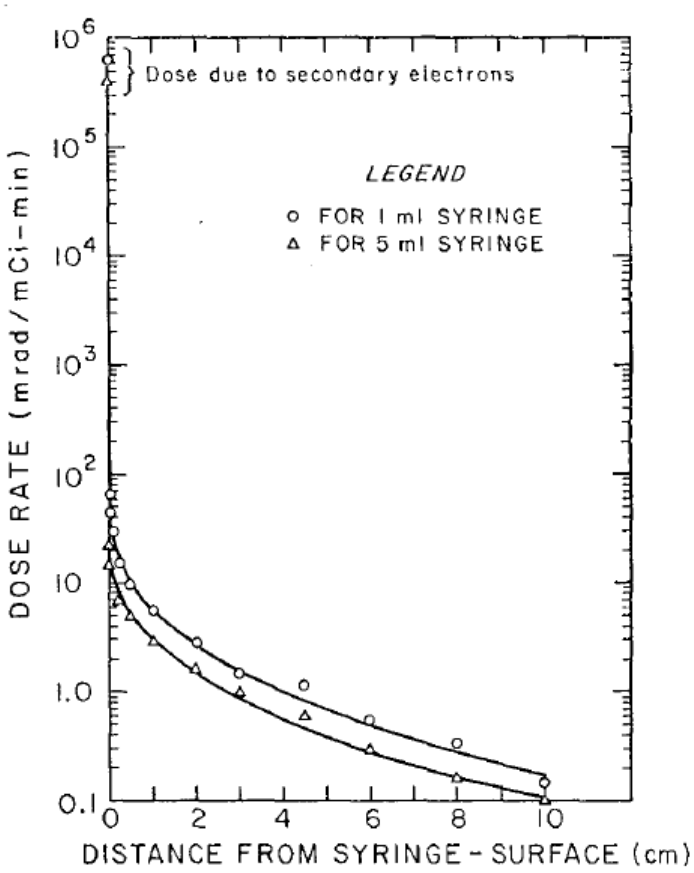

Figure 7: Radial Dose Rate for Tc-99m as a function of distance **(Tripathi, 1977)**

2.5.2 Accidental Worker Exposures

In a study by Saenger (1974), an compilation of case studies is presented where the absorbed dose has been forensically determined for accidental exposures of workers to high activity encapsulated sources. Various cases are presented where an individual was exposed to a source of known activity and duration. The dose is then assigned using dose conversion factors from NCRP-40, where the correction factor for secondary electrons is applied to the measured gamma ray dose rate. This publication is a demonstration of the importance of accurate dose assignment factors, such that a biological response is correctly attributed to a given exposure. Incorrect factors will cause the insult to be incorrectly quantified which may inhibit effective early treatment of the injury.

2.7 Summary

The case for examining the phenomena of secondary electron emission has been substantiated as the components of the emission intensity at the capsule surface are not well described in those references used in NCRP-40. In all publications reviewed, the size, shape, and material of the ionization chamber, as well as any differing geometries in the source, are identified as contaminating the resultant dose rate detected. The historical experiments are therefore only applicable for use as a relative comparison to other datapoints recorded in the same research study, and are not applicable to real biological effects, or as a quantification of the actual dose rate. Simulations executed using a numerical model will enable detection at the surface region of the source, without the sources of error present in the reference studies.

CHAPTER 3 METHODOLOGY

The experimental results obtained in this thesis were obtained via a numerical simulation model, with the objective to minimize qualitative and quantitative errors which affected the result of historical studies referenced by NCRP-40[4]. The individual experiments used as the basis for simulation are described herein, and are subdivided as follows:

1. Verification of the Monte Carlo simulation code with respect to accuracy and precision in reproducing a result from a physical trial. This is achieved by executing a simple trial, which was previously completed in a referenced historical study. This approach, using a historical reference, is required as new physical trials were not within the scope of this research.
2. Reproduction of source models from those models reference by NCRP-40, which are then simulated in MCNPX. Updated recommendations will be made based on any differences found.
3. Execution of simulation for the specific source model stated in NCRP-40 to obtain the dose conversion factors and secondary electron correction factors

The steps described above are further subdivided into an array of regions where the dose is sampled in the simulation. These regions are listed in Table 2 below:

Table 2: Test matrix showing regions evaluated for the source models simulated

Regions Evaluated	Models used in Simulation		
	1. Depth Dose Determination (Section 3.2)	**2. Secondary Electron Correction Factor (Section 3.3)**	**3. Surface Dose Rate (Section 3.4)**
Surface Dose Rate	●	●	●
Dose Rate at Discrete Depths in Tissue, up to 1mm			●

[4] See Chapter 2 of this thesis for a discussion regarding the historical reference studies.

Dose Rate for a Range in Tissue (0-1mm)			•

3.1 MCNPX Code Description

The numerical simulations completed as a part of this thesis were performed using the Monte Carlo N-Particle eXtended (MCNPX) transport code, Version 2.6.0 (Los Alamos National Laboratory, 2007). This is a general purpose code which is able to transport neutrons, photons and electrons, both singly or as a coupled simulation. The Monte Carlo method is based on a stochastic process, where the direction emission is random, and the probability of interaction is based on cross section data for the material and radiation type. The behaviour seen in Figure 8 is termed the random walk, where the transport equation is subdivided into steps. Within each step an interaction may occur based on the individual cross sections for each type of possible event.

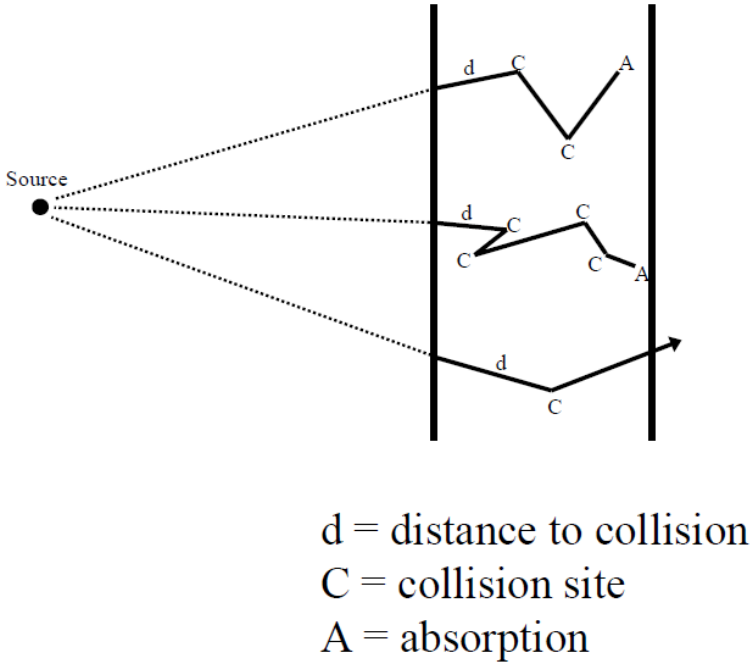

Figure 8: Random Walk and Interaction in a Generic Monte Carlo Radiation Transport Simulation (Waller, Winter 2011)

The probability of interaction is dependent on: the type of radiation being transported, the energy of that emission and the material within which it occurs. All of these parameters are specified by the user and MCNPX uses reference data libraries for the cross section values which are input based on those conditions. The probability of producing a reaction (or not) based on those library reference values. For additional information on the design and execution of a model in MCNPX see Appendix A of this thesis for a sample input file, and the reference manual for the code published by the Los Alamos National Laboratory (Team, 2003)

To obtain a value for the deposition of energy in a specified region, MCNPX tracks the history of the starting particle, and scores the resulting interactions until the energy of the starting particle reaches a minimum value, or escapes from the system. The secondary particles that are generated from the interactions also tracked, and the energy deposition resulting from subsequent interactions are also scored. Scoring is achieved by a tally functions in MCNPX, which is analogous to a detector in a physical apparatus, where the function and type of tally used in the simulations for this thesis is described in Section 3.1.1.

3.1.1 MCNPX Heating Tally

MCNPX is enabled to detect energy deposition from transported particles interactions via the application of a tally designation to a desired point location or cell geometry specified by the user. Simulations performed in this thesis use a F6 heating tally which is a "track length flux tally modified to tally a reaction rate convolved with an energy-dependent heating function" (LANL, 2005). That is, a geometry that is designated as a F6 tally will track the particles passing through it, where each particle entering the volume counts towards the score if an interaction occurs. Based on the type of particle, MCNPX applies a factor to account for the energy loss of that particle as it travels through the cell. The final result is a score value for energy deposition from primary and secondary radiation in units of MeV/g, which is absorbed dose.

The simulation model is designed to transport photons and electrons, and the tally is enabled to detect this emission by designating it F6e which tracks energy deposition from the electrons that result from primary photons. The histories of all particles are averaged and normalized to a starting particle, and this is the result that is stated for all results from the MCNPX simulations in this thesis.

Additional modifications are made in the code to increase the accuracy of the result and maximize computational resources. A constant factor was applied to the mass input for the F6 tally unit of (MeV/mass)/particle in the form of an SD card with value of 1. This card modified the mass of the detector cell to 1 gram, providing a result detector unit value normalized to a unit mass. The volume must be user defined and it was determined to be simpler to define this external to the code, thus the actual mass of the target geometry is factored in when converting the units obtained in the simulation to units of dose rate (Eqn 7).

To ensure that the transport and interaction of the emission was executed as accurately as possible, a detailed physics treatment was applied in the code for both photon and electron transport. This selection is made to ensure that low energy electrons from the Compton and Photoelectric effects are correctly modeled, and the fluorescent photons are transported[5]. This inclusion is critical as the expected emission will produce a large proportion of low energy photon and electron emissions in the detector region. Additionally the Integrated Tiger Series (ITS) Energy Indexing Algorithm is applied to the electron transport portion of the code. The difference between this designation and the code default setting is a reduction in the number of times that linear interpolation is performed on partial steps as the electron emission loses energy. This makes the ITS algorithm a more accurate representation of the slowing down physics for electrons, particularly at lower energy.

[5] See the MCNP user manual for additional detail (Team, 2003)

3.2 Depth Dose Determination and Verification of Simulation

To verify the MCNPX code used to simulate the models in this study, physical experiments should first be performed and then replicated as a simulation, where good agreement in the results would indicate the accuracy of the code in simulating the actual system. However, limitations of the scope of this research did not allow physical trials to be completed.

To perform the verification, a simple experiment was selected from the Quimby (1939) study, which is described in Section 2.4. A portion of that work examined the penetration depth, in water, of the secondary electrons generated from an encapsulated Ra-226 source, where the capsule material varied in each measurement but was of equal shielding thickness. Quimby demonstrated that after the penetration depth of 1mm by the principle gamma rays and secondary electrons in tissue equivalent material, the detected intensity was approximately equal for all trials. This indicates that the secondary electrons generated at the source surface are absorbed in the first 1mm of tissue, see Figure 9. After passing through 1mm of tissue equivalent, the net dose rates measured were within 7% of each other for source encapsulations of *Catalin (Z=6), Aluminum (Z=13), Copper (Z=29) and Gold (Z=79).

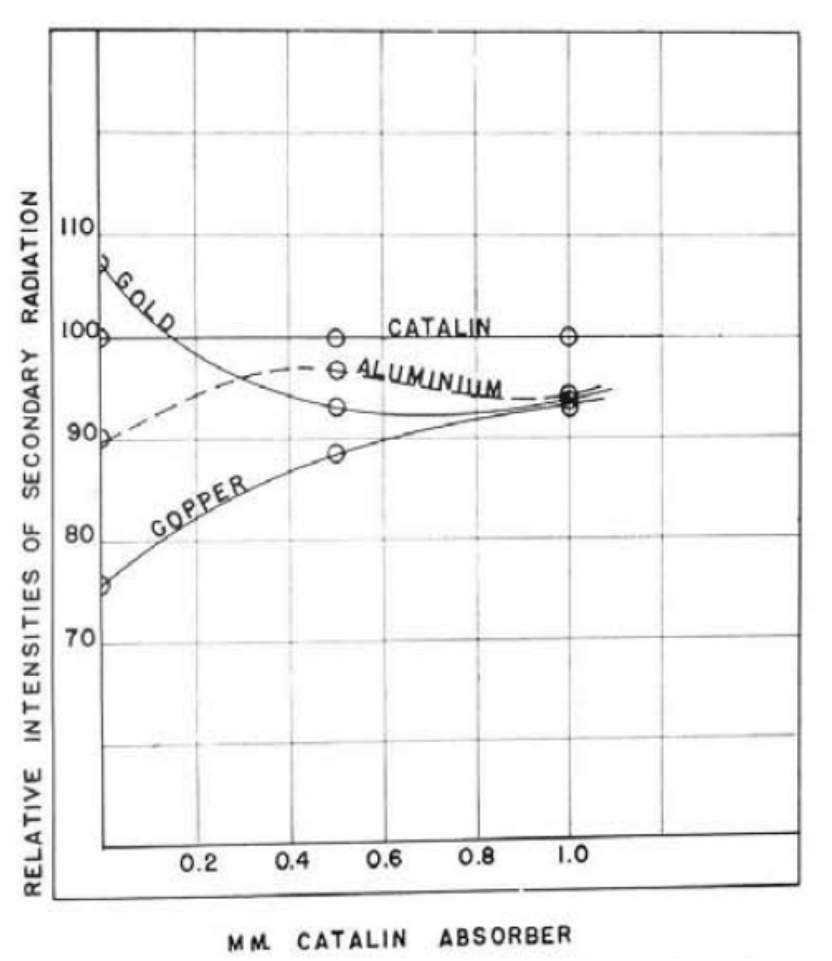

Figure 9: Relative intensity of secondary radiations after passage through 1mm tissue equivalent (Catalin), (Quimby, 1939)

*Catalin is a material with physical properties similar to celluloid. The composition of this material is stated by the manufacturers as: carbon 64%, oxygen 19%, hydrogen 5%, moisture 9%, ash 2% where the metal in the ash in predominantly sodium.

This result is ideal for verification as there is no relative difference when comparing the measured values, only comparison for symmetry of the results. Since equivalent shielding thicknesses are well documented, the sources of experimental uncertainty are acceptably low, permitting the use of this experiment for the basis to verify the simulation method.

The Quimby apparatus is similar to that used by Benner (1931), and thus the model dimensions are the same for continuity purposes. The detector used in the model is a very thin tissue equivalent layer

encompassing the penetration tissue layer, and is designed to measure the energy deposition from all photon and electron radiation. The detector encased the source and the 0.1 cm penetration tissue layer, and was of 0.007 cm depth, (Figure 10).

All other dimensions for the source and encapsulation thickness equivalent to the Benner (1931) apparatus where the diameters of the sources are: Catalin (Z=6) at 0.45 cm, Aluminum (Z=13) at 0.21 cm, Copper (Z=40) at 0.079 cm, and Tungsten (Z=74) at 0.036 cm. The encapsulation dimensions are of equivalent shielding thickness. The Benner (1931) apparatus is fully described in Section 3.3, Figure 11.

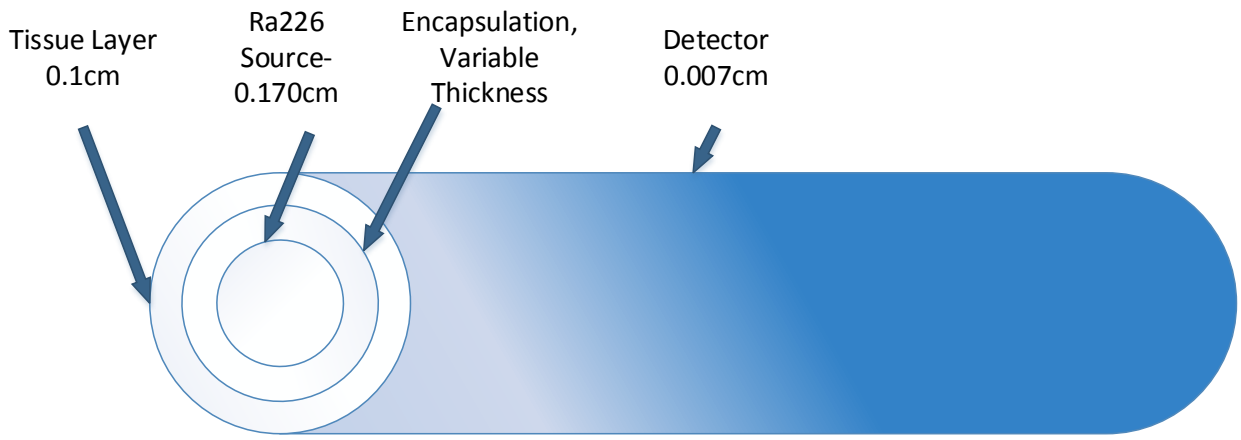

Figure 10: Source Model, Depth Dose Simulation

From the results of this simulation, the relative difference of surface emission was determined for encapsulation materials: Catalin, Aluminum, Copper, and Tungsten. Dose rate values were obtained from the detector layer in units on MeV/g and are described further in Chapter 4.

3.3 Secondary Electron Correction Factor

The study by Benner (1931) used an apparatus designed to evaluate the secondary electron component of the emission generated in a capsule wall for a Ra-226 gamma source. As the secondary electron component of the emission is required to generate a correction factor for secondary electrons, thus the Benner (1931) study is the primary reference for the correction factors proposed in NCRP-40, as all other references only evaluate the relative aspects of total surface emission.

To assess the accuracy of this result, the source was modelled and simulated in MCNPX. The apparatus used in that experiment measures the total and photon only emission from encapsulated source models as a function of capsule material of equivalent shielding thicknesses. Detection is via an ionization chamber, and an electro-magnet is used to deflect the secondary electron emission allowing detection of gamma rays without contribution from electrons.

The simulation values obtained are shown using the ratio of the total emission to photon only emission, which is displayed for increasing atomic number encapsulation materials. Other references cited in NCRP-40, with respect to this phenomenon (Shalek, Stoval, Attix, & Tochilin, 1969) (Quimby, Marinelli, & Blady, 1939), publish data that did not incorporate the components of the beam and therefore were not able to determine the secondary electron correction factors

The source model from Benner (1931) was reproduced in MCNPX to replicate the results found in that study, and is described below (Figure 11):

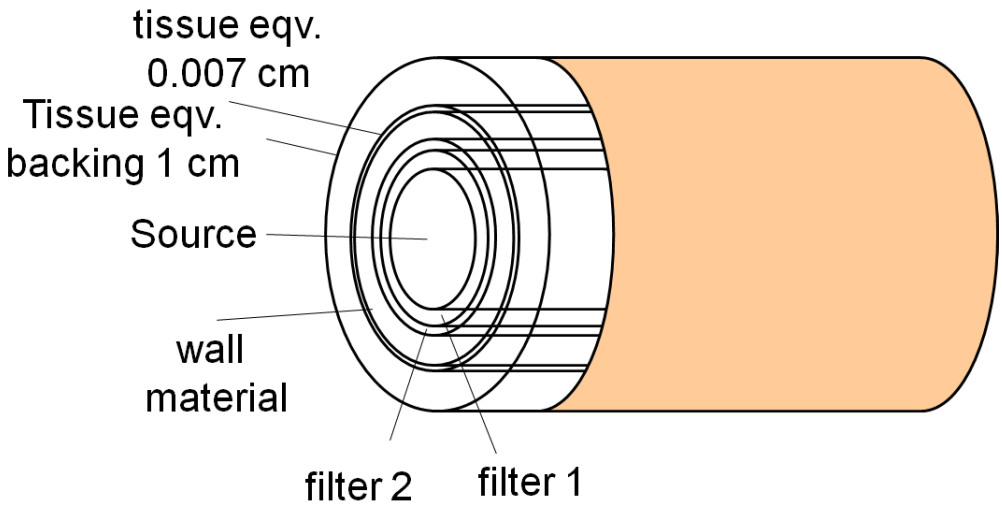

Figure 11: Source Model, Secondary Electron Emission as a function of material – (Benner,1931)

The MCNPX source capsule model is faithful representation of the Benner (1931) model. The source is Ra-226 with dimensions of 0.170 cm diameter and 0.34 cm length. The source was then encased in a primary container of gold (Au) and a secondary filter of platinum (Pt) of thickness 0.035 cm and 0.03 cm. Encasing the source and filters is a capsule of varying material thicknesses designed to filter the secondary radiation emitted from the filters. Thicknesses are of equivalent shielding thickness and are selected at intervals such that samples are represented over a range of atomic numbers 6-79.

The detector ionization chamber was not necessary to reproduce in the simulation, as MCNPX utilizes a tally type detector function. Similarly, a magnetic field was not employed in the code, nor could it be, as the capacity is not included in the software, however the gamma ray dose was isolated by setting the wall

region to a null importance with regard to electron transport. This setup allowed only photon transport to occur past the designated boundary, and thus achieved the function of a 100% efficient electron filter.

To detect the emission at the source surface, a layer must be designated as the detector to evaluate the photon and electron ionization in that region of interest. This region was not accurately assessed by Benner as shown in Section 2.3. However as NCRP-40 states the results published apply to the surface region, this is the region that is evaluated in the simulation.

Since NCRP-40 states values for the surface conditions, the simulation is bound to model this condition, regardless of the actual measurement method used by Benner. The detector region in the simulation is applied a tissue layer encasing the source and capsule of thickness 0.007 cm which is adequately thin in order to evaluate the surface condition approximately. A backing layer of tissue equivalent material depth of 1.0 cm is applied to simulate interstitial use of the source. This model is referred to as Variation 1 (Figure 11). While it is not imperative to reproduce the Benner (1931) result exactly, it is desirable to understand if there is any deviation found in the simulation in order to better understand the secondary electron conversion factors stated in NCRP-40.

To obtain data from the simulation which will have a higher probability of conforming to that obtained by Benner, a model for simulation would have to be designed to capture emissions over the total range of the secondary electrons. This type of model will more closely reflect the conditions present in that study, see Section 2.3. This was achieved by designated the detector to increased thickness 0.1 cm, which is the maximum range for secondary electrons in tissue generated by the source models studied in this thesis. The model was executed with this arrangement, and the photon only and total dose rates were evaluated

in that region in the same manner as in Variation 1. This MCNPX model is titled Benner (1931) Replication – Variation 2, and is discussed in Section 4.3.

3.4 Surface Dose Rate Calculation

Following the verification of the simulation code and the reproduction of the data used for the secondary electron correction factors, the source model described in NCRP-40 (1972) was modelled and executed per the steps in the test matrix, see Table 2. The source model is described in NCRP Report No. 40 – Table 7 (of that publication) (NCRP, Protection Against Radiation from Brachytherapy Sources, 1972) titled "Approximate Gamma Ray Dose to the Hand for 1 Curie in a sealed source", also see Table 1. Described in the tables are the contact surface dose rates for Radium-226, Iridium-192, Caesium-137, and Cobalt-60, encapsulated in stainless steel (type 304), of thickness 1/32inch.

The axial dimension of the source model was assumed to be 1 cm. The NCRP-40 report approximates the cylindrical geometry as a point source, however to increase the realism of the simulation an axial dimension is applied. To ensure the continuity of this simulation to those historical studies described (section 2.3), the source model described in the in Depth Dose Verification, Section 3.1 was used as a framework for the NCRP-40 model, (Figure 10). Changes to that model were required to align the parameters to the sources described in the report. This was the material of the encapsulation updated to Stainless Steel 304 thickness 1/32 inch, with outer diameter equal to ¼ inch.

The dose rate was measured at the surface of the source and at increasing intervals from the surface through the tissue equivalent material from 0 cm to 0.1 cm. The was achieved by the application of a very thin detector layer of 0.007 cm at the desired distance from the source, see Table 2. The

measurement at the source surface is the value comparable to the surface dose rates stated in NCRP-40, while all other values measured at increasing distance are designed to demonstrate the decreasing contribution of secondary electrons as the measurement location increases radially from the source.

3.4.1 Depth Dose Region Simulation

The source model used in Section 3.4 was also applied to addition trials to determine the dose rate at a depth ranges in tissue up to 0.1 cm from the source surface. This method is applicable to an external exposure scenario as described in the Tripathi (1977) study, but is not explicitly referenced in the NCRP 40 report. The justification of the additional simulation is two part: surface dose rates stated in the report are not applied to an external exposure scenario as there is no compensation for dose reduction in the epidermal layer, and second dose attribution must consider the entire range of tissue affected by secondary electron emission which extends beyond the conditions at the immediate surface.

In this simulation, three regions were simulated to obtain an average dose rate in the regions of interest: 0-0.01 cm, 0.01-0.1 cm, and 0-0.1 cm, which correspond to: the region of highest dose near surface, the region of active tissue in the sub-dermal layer (for external dose applications), and the total travelled path length of the secondary electron radiation, applicable to internal exposure applications.

CHAPTER 4 RESULTS and ANALYSIS

4.1 Depth Dose Determination

Depth dose verification was the first model simulated as a verification of the MCNPX code. Depth dose experiments were performed by Quimby (1939) that showed total emission strength detected for sources of different shielding materials were within 7% after passage through 1mm in tissue. This result also confirms the range of the secondary electron radiation produced from encapsulated Ra-226 sources.

4.1.1 Results

The expected result is that the emission intensity at the boundary of 1mm tissue depth will be approximately equal for a Ra-226 source encapsulated by different materials of equivalent shielding thickness. This equivalence is shown by comparing the total dose value for each capsule material to the first, to the total dose for capsule material Z=6. The intention is that the data within the set should be approximately equal, and thus one data point is selected for the comparison of all the others. It is not critical which point is selected, Z=6 is chosen here for continuity with the parent experiment, Quimby (1939). The data from the simulation is seen below in Table 3:

Table 3: Total Energy Deposition at 1mm Tissue Depth Boundary – Simulation data

Capsule Material (Z)	Reference Value	Total Dose (Mev/g)	Fractional Standard Deviation (FSD)	Difference (%)
6	1.30E-04	1.30E-04	0.0116	0
13	1.30E-04	1.28E-04	0.0114	1.5
40	1.30E-04	1.31E-04	0.0117	0.8
79	1.30E-04	1.23E-04	0.0118	5.7

As seen in Table 3, the percent difference between the total emission is <6%, which is in good agreement with the result from Quimby which recorded <7% over all trials (Quimby, Marinelli, & Blady, 1939).

4.1.2 Analysis

The result confirms the finding by Quimby that after passage through 1mm of tissue, the emission intensity from an encapsulated Ra-226 source at the surface is not dependent on the shielding material of the capsule, given equivalent shielding thickness. Thus, the energy maximum of the secondary electron is limited to a range of 1mm for an encapsulated Ra-226 source, which provides a bounding region of interest for future analysis.

Critically, this result demonstrates that the particle energies simulated are in good agreement with those from the Quimby experiments. Thus, a simulation using the MCNPX code with a F6e heating tally is seen to precisely reproduce the results of a physical experiment. From this, additional simulations of secondary electron generation and emission can be completed with confidence that the results will be equally accurate.

The dataset in Table 3 is used as a means of substantiating continued simulations in this study, and demonstrates the value of the total travelled path length for secondary electron radiation from an encapsulated Ra-226 source. This range value is used to limit the future trials to the effects observed within 1mm of the source surface in tissue material.

4.2 Replication in MCNPX

A model of the apparatus from the study by Benner (1931) was simulated as a part of this thesis to determine the component of the emission from secondary electrons. The isolation of the electron emission permits the calculation of the correction factor for the measured gamma ray dose from an encapsulated source, which is the basis of the correction factors stated in NCRP-40 (Table 1). Results of this simulation are displayed to show the secondary electron correction factors for the source models described in Section 3.3

4.2.1 Result - Variation 1

The model seen in Figure 11 was simulated using the method described in Section 3.3 to isolate the secondary electron emission. This is the Variation 1 simulation, and the results are shown in Table 4, and Figure 12.

Table 4: Total and Photon Only Dose Rates - Simulation Data, Variation 1

Z#	Photon Only Dose Rate, (MeV/g)	Photon Only FSD	Total Dose Rate (MeV/g)	Total FSD	Ratio
6	2.75E-05	2.42E-02	1.63E-04	1.10E-02	5.95E+00
13	2.65E-05	2.48E-02	1.50E-04	1.22E-02	5.66E+00
22	2.80E-05	2.36E-02	1.32E-04	1.07E-02	4.71E+00
29	3.15E-05	2.36E-02	1.45E-04	1.07E-02	4.62E+00
40	3.67E-05	2.43E-02	1.46E-04	1.24E-02	3.98E+00
50	3.91E-05	2.43E-02	1.76E-04	1.24E-02	4.51E+00
58	3.86E-05	2.43E-02	1.93E-04	1.24E-02	5.01E+00
65	3.63E-05	2.51E-02	2.11E-04	1.03E-02	5.82E+00
74	2.41E-05	2.51E-02	2.21E-04	1.03E-02	9.17E+00
82	2.46E-05	2.08E-02	2.57E-04	7.60E-03	1.04E+01

This data shows the ratio between the photon dose and the combined dose, which includes the secondary electron emission for materials of increasing atomic number. It is seen that the secondary electron dose component is 3-9 times greater than the dose from gamma for capsule materials of increasing atomic number.

The differences between the simulation data and that obtained by Benner (1931) are in excess of an order of magnitude in the most extreme case, where the Benner data can be seen in Table 5. Error terms for the data there are not included in that publication and are thus not shown in the table. Distinct variations between the simulation data and the reference publications are noted as follows:

1. The values obtained from the simulation generally exceed those from Benner (1931) for all encapsulation materials.
2. At the highest atomic number encapsulations the simulation data exceeds general trend, (Figure 2), where the emission maxima occur approximately equal at the lower and higher atomic number encapsulations.

Table 5: Relative Dose Contributions for varying Encapsulation Material – Historical Study, Benner (1931)

Capsule Material (Z)	Electron Emission Intensity (charge, I_e)	Photon Emission Intensity (charge, I_o)	Ratio	Secondary Electron Correction Factor
7	11.53	10.80	2.07	106.78
13	9.37	10.80	1.87	86.72
26	6.42	10.80	1.59	59.48
28	6.58	10.80	1.61	60.92
29	6.50	10.80	1.60	60.20
29	6.81	10.80	1.63	63.07
30	6.58	10.80	1.61	60.92
30	6.35	10.80	1.59	58.77
47	6.42	10.80	1.59	59.48
50	6.42	10.80	1.59	59.48
82	10.38	10.80	1.96	96.15

The data obtained from the Variation 1 simulation indicates that the surface dose rate would be understated in the physical trials for all encapsulation material. This would result in incorrect correction factors and dose conversion rates as described in NCRP-40.

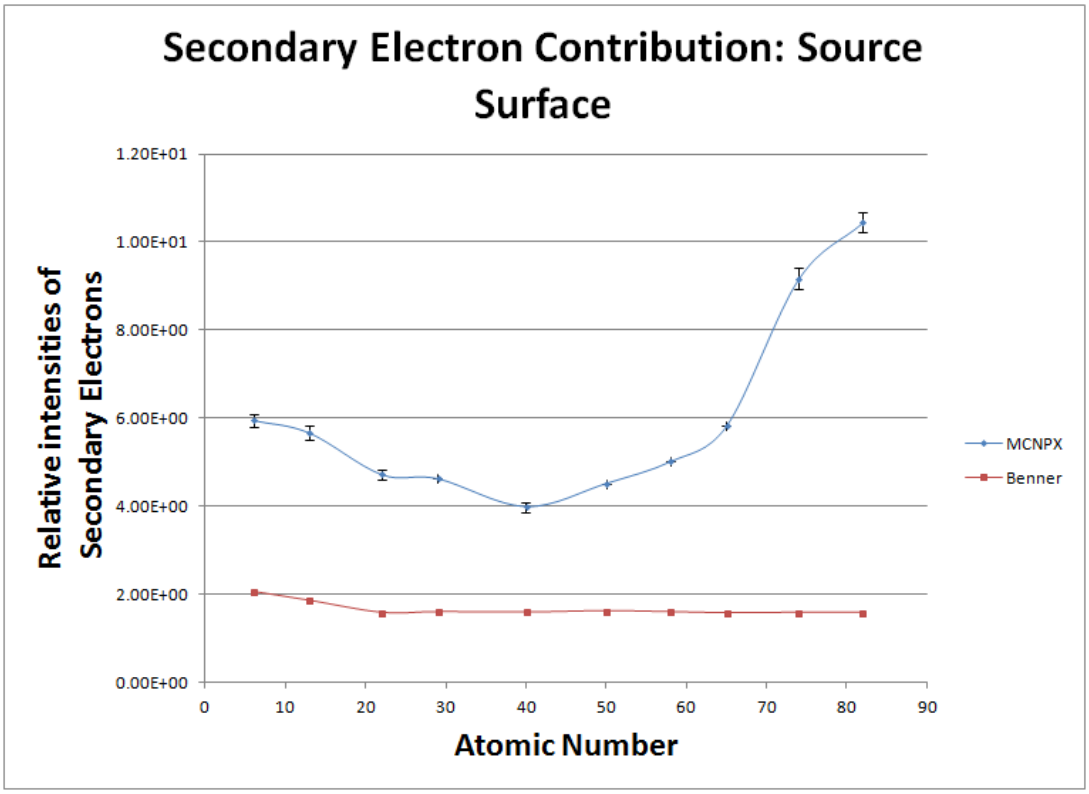

Figure 12: Relative intensity of secondary electron radiation as a function of encapsulation material (Simulation in MCNPX – Trial: Variation 1)

The additional region of interest occurs at the highest atomic number encapsulation values, those greater than Z=58. The expected trend is that, as atomic number of encapsulation increases, the emission intensity increases past the minimum due to the additional contribution from the Photoelectric Effect (Baratta & Lamarsh, 2001). The trend in Figure 12 shows a sharp increase in the simulation data with respect to historical data set from Benner, observed at the higher Z values, which suggests that a majority component of the secondary electron is being generated for this type of source configuration, as

described in Section 1.2. This effect was not detected in those historical radium studies due to a lack of sensitivity in the detectors available[6].

Despite from the deviation identified above, the simulation data and that obtained in the historical studies follow roughly the same gradient between series data as a function of capsule material. Both of these differences are seen clearly in Figure 12 and are discussed in the following Section 4.2.2.

4.2.2 Analysis - Variation 1

The radium studies cited by NCRP-40 were reproduced in MCNPX as described in Chapter 3. Reproduction of the source data allowed the calculation of correction factors for secondary electron emission from simulation values, which are comparable to those stated.

The simulation results were obtained by executing the source model using a 0.007 cm depth tissue equivalent detector to evaluate the condition at the source surface. The shallow detection depth evaluates less than 1% of the total range for the secondary electrons emitted. This design allows a snapshot type assessment of the emission at the surface region, capturing the initial interactions at the capsule surface before any slowing or attenuation has occurred. The data is then compared with the historical radium study data, which did not to evaluate the emission at the source surface without eliminating all distortions and error in the measurement. The result from the simulation data is thus expected to exceed the numerical magnitude and the accuracy of the physical trials due to the difference in detection methods.

[6] See Section 2.2 and 2.3 of this thesis for an expanded explanation of the historical apparatus.

The simulation data for Variation 1 is shown in Table 4 and Figure 12, Section 4.2.1. Figure 12 shows the relative intensity of the secondary electron emission, which is a ratio used to determine the proportional contribution. Poor agreement is observed in the comparison between the simulation and the historical data, with the simulation results higher by 5-10 times. While the difference in absolute values is significant, the trend follows the pattern seen in the historical studies for an increase/decrease in secondary electron emission as the capsule material changes. That is, the gradient between and two data points is approximately the same for the simulation data as it is for the historical study. This is shown in Figure 13 below, where the entire simulation data set has been reduced by a common numerical factor of 2.88 to align the both data points at Z=6, where it may be observed that the simulation curve follows the gradient seen by Benner, up to encapsulation material values of about Z=58.

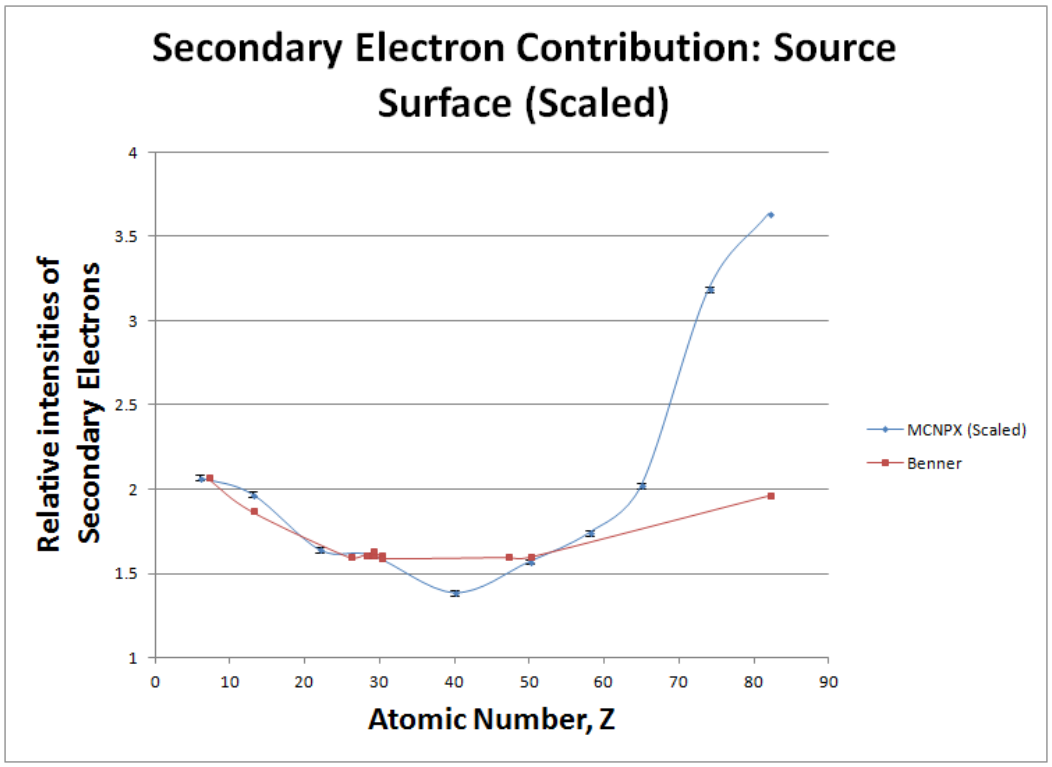

Figure 13: Relative intensity of secondary electron radiation as a function of encapsulation material – Scaled (Simulation in MCNPX – Trial: Variation 1)

As the encapsulation material exceeds approximately Z=58, the proportional contribution of the secondary electrons increase beyond that measured in the historical radium trials, and thus poor agreement is seen between the simulation and published data. The rational for this deviance is due to the apparatus used by Benner (1931) which was unable to detect the lowest energy secondary electron emission. The production of lower energy secondary electrons increases for gamma ray interactions at high Z materials due to the increased photoelectric cross section. For high Z materials, more orbital electrons are present with lower binding energies, thus gamma rays which have been attenuated in the source and capsule material are now able to induce ionization, which did not occur at lower Z encapsulation material. For an expanded explanation on this phenomena, see Section 3.8 of (Baratta & Lamarsh, 2001). The consequence of this deviation is that a correction factor for a high Z material using the Benner (1931) data would incorporate the highest inaccuracy for all the material encapsulations examined.

The simulation data trend described above is confirmed in a by an semi-good correlation in the historical study by Quimby (1939). The apparatus used in that experiment was also subject to the aforementioned inaccuracies. However, the design allowed a more accurate accounting of the surface emission than the Benner (1931) trials, where the differences in the detector setups can be seen in Section 2.3 – 2.4. Quimby found as the encapsulation material increased past Z=60, the emission intensity increase rapidly surpassing the measured value at Z= 6, which is not in agreement with the Benner trend, but does qualitatively agree with the simulation (Figure 4 and Figure 12).

An additional qualitative correlation between the historical radium studies and the simulation data from Variation 1 can be observed in the results of exposure trials performed by Quimby, described in Section 2.4. In those trials, encapsulations of Catalin (Z= 6), aluminum, copper, and tungsten were applied to live

human tissue (upper arm), and the reaction over time was assessed for severity of erythema. The most pronounced reaction was observed for the tungsten encapsulation for exposures of equal duration from all sources, which corresponds to the highest Z material encapsulation for all test cases.
This region of increase is missing from the trend found by Benner, and is subsequently excluded from the trend summarized by Attix (1969) (Figure 2). The tissue reactions found by Quimby (1939) support the simulation data found in Variation 1 (Figures 12 and 13).

The partial discrepancy in the Variation 1 simulation data, and Quimby (1939) is attributed to the added accuracy in the numerical simulation which also eliminates the error terms associated with the analog apparatus. The discrepancy with respect to Benner (1931) exists for similar reasons and is more pronounced as the detector used was less accurate than both of the above when considering the emission intensity at the source surface.

This result is significant when selecting materials to be used as a capsule to contain a gamma source, as well as generic gamma ray shielding applications where the shield may come into contact with personnel. The historical studies will underestimate the surface dose rate at the high Z value (Z=65-82) encapsulations by a factor of 10, with the other encapsulation materials underestimated by 3-6 times.

As the data obtained in the Variation 1 simulation is in poor agreement with Benner (1931), and only qualitative agrees with Quimby (1939), an additional simulation was performed as a part of this thesis to replicate the inaccuracies that were present in the historical radium trials. This additional simulation is designed to show how much (or little) of the emission spectrum was actual recorded by the detector used by Benner (1931). From this result a recommendation may be provided on how that historical data may be accurately applied.

An evaluation of the detector used by Benner (1931) shows that the ionization chamber used was of a large volume relative to the range of the radiation. It is likely that the multiple interactions were recorded as the emission lost energy through the chamber, and it is equally plausible that the secondary electron energy is completely deposited there. To test this hypothesis a modified model was constructed and executed under the title "Variation 2". The changes were applied to the Variation 1 model, where the detector target layer thickness is increased to 0.1 cm. This increased thickness corresponds to the approximate range in tissue of the secondary electron emission from an encapsulated Ra-226 source. The object of the Variation 2 simulation is to replicate the detector conditions in the apparatus used by Benner, with the expectation that a similar experimental result will be found.

4.2.3 Result – Variation 2

Due to the large difference between the Variation 1 data and the Benner (1931) trend, an additional model was designed to emulate the conditions of that apparatus. This was achieved by measuring the dose rate over the entire range of the secondary electrons in tissue, which was found to be approximately 1mm in Depth Dose Verification, see Section 4.1. This model is titled Variation 2, and the goal of this simulation is to produce results that are similar to those from Benner (Table 5), by enabling detection of the emission from the surface for the entire range of the secondary electron emission. Successful reproduction will confirm the hypothesis that the Benner (1931) apparatus measured the source emission over a range.

The range over which Benner measured the emission is not precisely known, and conservatively the entire range of the secondary electron must be included in the detector region for the simulation. This range is 1mm in tissue as shown in the study by Quimby (1939) and Section 4.1 of this work. As the secondary electron emission likely did not deposit all energy in the detector, the results from the Variation 2 simulation are expected to be marginally higher than those from Benner. However this discrepancy is

acknowledged and will be factors into the analysis of the results. The Variation 2 simulation is based on the Variation 1 design, with a change to detector cell thickness which was increased to 0.1 cm from 0.007 cm (Figure 11).

The method for executing the simulation for Variation 2 was exactly as Variation 1, and trials were completed with encapsulations materials from atomic number 6 to 82. The data is listed in Table 6, and shown in Figure 14.

Table 6: Dose rate in tissue layer 0 - 0.1cm, for varying material encapsulations – Simulation data, Variation 2

Atomic number	Photon Only Dose Rate (MeV/g)	Photon only FSD	Total Dose Rate (MeV/g)	Total FSD	Ratio (Figure 14)	Secondary Electron Correction Factor
13	1.26E-03	6.5E-03	2.25E-03	5.7E-03	1.78E+00	78.04
22	1.26E-03	6.4E-03	2.06E-03	5.7E-03	1.64E+00	63.98
29	1.28E-03	6.3E-03	2.11E-03	5.7E-03	1.64E+00	64.35
40	1.24E-03	6.2E-03	2.08E-03	5.8E-03	1.68E+00	68.48
50	1.21E-03	6.3E-03	2.11E-03	5.8E-03	1.73E+00	73.31
58	1.20E-03	6.3E-03	2.20E-03	5.7E-03	1.83E+00	82.82
65	1.17E-03	6.4E-03	2.23E-03	5.6E-03	1.90E+00	90.19
74	1.14E-03	6.5E-03	2.31E-03	5.4E-03	2.02E+00	102.02

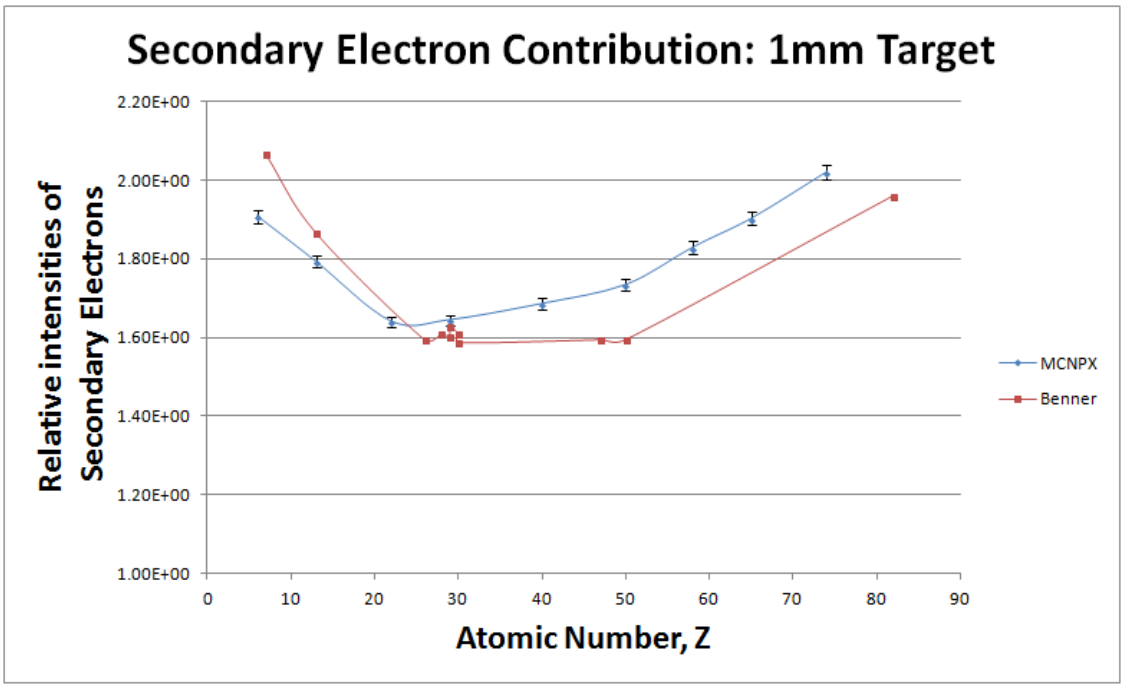

Figure 14: Relative intensity of secondary electron radiation as a function of encapsulation material (Simulation in MCNPX – Trial: Variation 2)

4.2.4 Analysis - Variation 2

The proportional emission of the secondary electron emission for encapsulations of increasing atomic number is compared with the data published by Benner, (Figure 14) (Table 5). The overlaid trends in Figure 14 are in good agreement, with a maximum difference of approximately 10%.

This result confirms the hypothesis that the data obtained in Benner (1931) and other publications summarized by Attix (1969), and cited by NCRP-40, are only applicable to total the secondary electron a range in tissue, and not the discrete boundary of the surface. Surface dose rate conclusions based upon this dose averaged over a layer of tissue will underestimate of the proportion of secondary electrons at the surface, which is an incorrectly low correction factor for secondary electrons.

Additionally, the simulation shows that the Benner experiments did not detect the lowest energy secondary electrons near the source surface. This is shown in simulation values, which slightly exceed those of Benner at the highest atomic numbers, see Figure 14.

The overall good agreement seen in Variation 2 with the Benner (1931) result establishes the model design parameters required to accurately simulate the radioactive energy deposition over a range near the surface, and also provides the rational to the hypothesis that Benner (1931) was not able to accurately measure source surface emissions.

4.3 Dose Conversion Factors

NCRP-40 states surface dose rates for an encapsulated Radium-226 source with a correction factor recommended for the additional contribution from secondary electrons, resulting in a total dose conversion factor. The surface dose rate in the report is based on a calculation of the gamma emission and the correction factors for secondary electrons based on research conducted by Benner, and Quimby.

The goal of this simulation is to obtain the dose conversion factor for surface gamma emission, for all encapsulated source models stated in NCRP-40. Where for a given gamma dose rate, the correction factor for secondary electrons may be applied as a multiplier, to obtain the total absorbed dose from a contact exposure. Enhancements found in the simulation results will be used to propose updated dose conversion factors. Additional simulations are performed to obtain dose conversion factors for increasing distance from the source through tissue. The goal of the additional analysis is to demonstrate the decreasing contribution of the secondary electron emission with respect to increasing depth in tissue.

4.3.1 Results

The simulation of the NCRP-40 source model was executed as described in Section 3.4, where the radioactive emission at the surface of an encapsulated Ra-226 source was assessed by a detector layer of tissue equivalent material 0.007 cm thickness. Additional sources listed in NCRP-40 are: cobalt-60, caesium-137, and iridium-192.

From the analysis of the simulations in Section 4.1 and 4.2 of the Benner replication trials Variation 1 and 2, the expectation of this simulation is that a similar difference will be shown, where the absolute values measured from the simulation will exceed that from NCRP-40. Differences in secondary electron emission

will be converted into updated correction factors for secondary electrons and subsequent updates to the total dose conversion factor.

The model design is based on the specifications described in NCPRR 40, (Section 3.4), and was simulated in MCNPX to obtain the total surface dose rate value, and the photon and secondary electron components of the beam, enabling a correction factor to be calculated. Results are shown in Table 7, where the first row of data is the emission condition at the surface of a stainless steel encapsulated Ra-226 source, with a secondary electron correction factor of 397%, which is comparable to the correction factor stated in NCRP-40 for that source type.

To understand the evolution of the emission intensity decrease as distance through tissue increases, additional trials were executed for detector locations at depths of 0.01 cm, 0.02 cm, 0.04 cm, 0.06 cm, 0.08 cm, 0.1 cm through tissue. (Table 7, Figure 15 and 16).

The units of Mev/g obtained by the simulation result are converted to units of R/min Ci based on an assignment of a 1Ci activity and using the following conversion terms:

$$\boldsymbol{Dose\ Rate}\left(\frac{\boldsymbol{R}}{\boldsymbol{min}}\right)\boldsymbol{Ci} = \frac{\boldsymbol{MeV}}{\boldsymbol{g}} \times \frac{\boldsymbol{Joule}}{\boldsymbol{Mev}} \times \frac{\boldsymbol{g}}{\boldsymbol{kg}} \times \frac{\boldsymbol{decay}}{\boldsymbol{s}} \times \frac{\boldsymbol{gamma}}{\boldsymbol{decay}} \times \frac{\boldsymbol{sec}}{\boldsymbol{min}} \times \frac{\boldsymbol{R}}{\boldsymbol{Gy}} \qquad \textbf{Eqn(7)}$$

Table 7: Dose Rate as a Function of Depth in Tissue – Simulation data, NCRP-40 Source Model

Detector Depth in tissue (from surface)	Total Dose (MeV/g)	Total FSD	Electron Only Dose (MeV/g)	Electron Only FSD	Secondary Electron Correction Factor
0.007	2.08E-04	4.0E-03	1.66E-04	2.0E-02	397.60
0.01	1.88E-04	1.1E-03	1.10E-04	1.9E-02	142.88
0.02	1.83E-04	1.1E-03	7.73E-05	1.8E-02	72.92
0.04	1.83E-04	1.1E-03	7.73E-05	1.8E-02	72.92
0.06	1.86E-04	1.1E-03	6.89E-05	1.7E-02	58.88
0.08	1.90E-04	1.1E-03	6.46E-05	1.6E-02	51.68
0.1	1.90E-04	1.1E-03	5.92E-05	1.6E-02	45.12

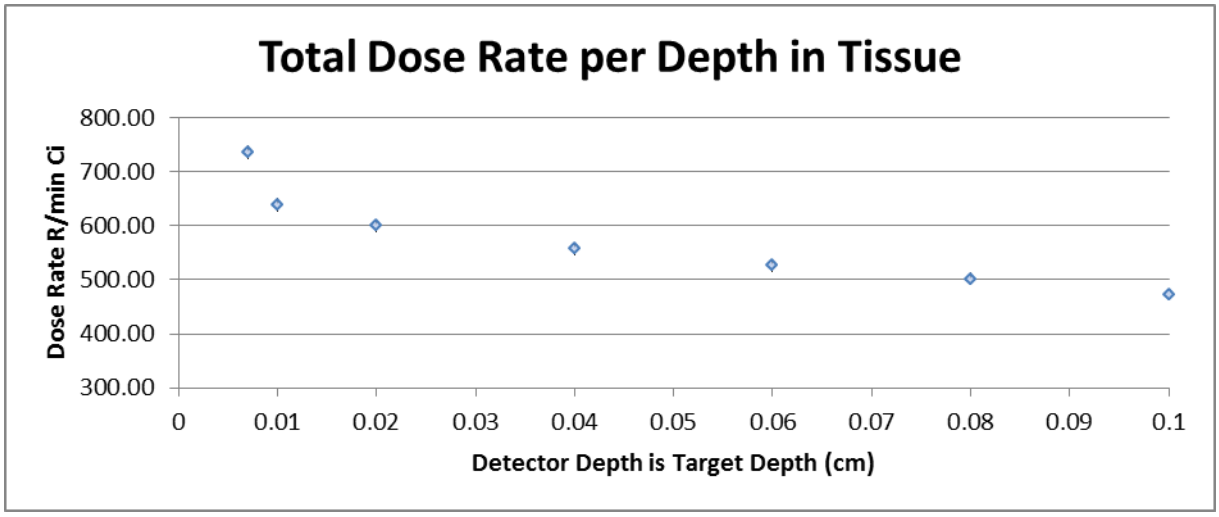

Figure 15: Total dose rate at discrete depths in tissue equivalent material – Simulation Data, NCRP-40 Source Model

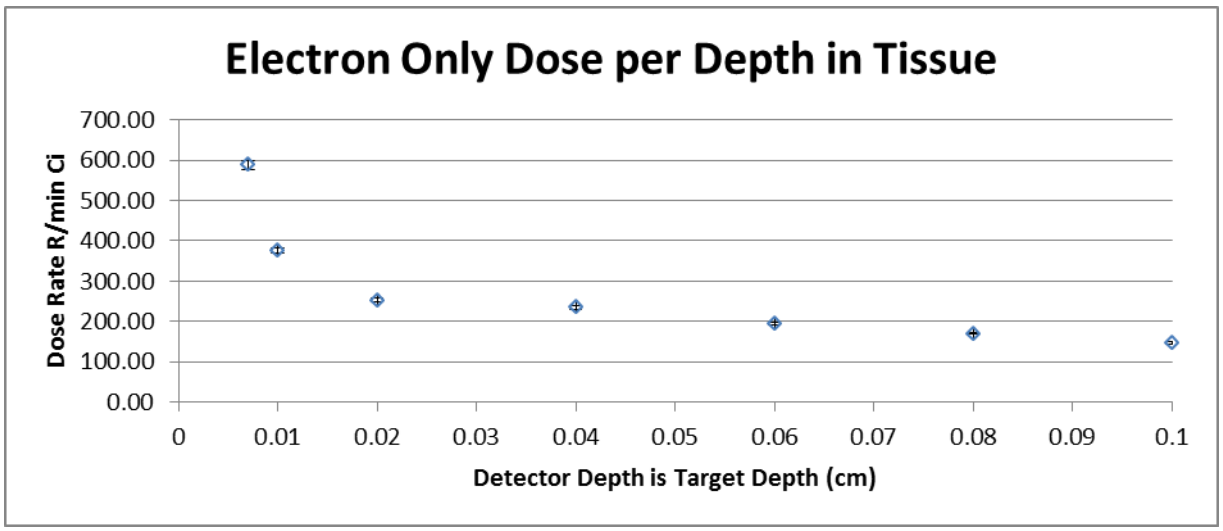

Figure 16: Electron Only dose rate at discrete depths in tissue equivalent material – Simulation Data, NCRP-40 Source Model

Figures 15 and 16 trend the simulation of the NCRP-40 source model, where the values of the highest dose rate occur at the distance nearest to the source surface, followed by an exponential decrease and plateau as the detector location from the source begins to exceed the range of the secondary electron radiation from the capsule. This behavior is in good agreement with the studies by Quimby and Tripathi for dose rates measured at discrete distances radially increasing from the source surface (Quimby, Marinelli, & Blady, 1939), (Tripathi, 1977).

The simulation data for the NCRP-40 Dose Conversion Factor simulation is compared to the data from NCRP-40 in the following subsections:

1. Table 8 shows the simulation photon only data, the secondary electron correction factor and the resultant total dose rate.
2. Table 9 shows the NCRP Report No. 40 data for: photon only, the secondary electron correction factor and the resultant total dose rate.
3. Table 10 shows the secondary electron correction factor for the simulation and NCRP-40 and the percentage difference between them.

Table 8: Dose Rate Data for Surface Dose Rates, Simulation Data, NCRP-40 Models

Radionuclide	Photon Dose (R/min-Ci)	Photon Dose FSD	Total Dose (R/min-Ci)	Total Dose FSD	Secondary Electron Correction Factor (%)
Ra-226	211.82	2.0E-02	1054.02	3.6E-03	397
Co-60	149	2.0E-02	1074	3.6E-03	620
Cs-137	82	2.0E-02	320	3.6E-03	290
Ir-192	109	2.0E-02	335	3.6E-03	207

Table 9: NCRP-40 Reference Data for Surface Dose Rates

Radionuclide	Photon Dose (R/min-Ci)	Total Dose (R/min-Ci)	Secondary Electron Correction Factor (%)
Ra-226	1310	1900	45
Co-60	2075	3008	45
Cs-137	513	743	45
Ir-192	813	1179	45

Table 10: Comparison of the Secondary Electron Correction Factors, Published with Simulation

Radionuclide	NCRP40 Secondary Electron Correction Factor (%)	MCNPX Secondary Electron Correction Factor (%)	Difference (%)
Ra-226	45	397	780
Co-60	45	620	1277
Cs-137	45	290	544
Ir-192	45	207	360

4.3.2 Analysis

The simulation results for secondary electron correction factors (Table 10) show poor agreement with the values published in NCRP-40, as seen in the percent difference column. The difference is in excess of 12 times for the most extreme instance for the Co-60 source. The difference for the Ra-226 source is 7.8 times, where the simulation exceeds the publication data.

The total surface dose rate for the Ra-226 source was measured to be 1054 R/min Ci in the simulation which is lower than that stated in NCRP-40 of 1900 R/min Ci, a difference of 80%. This result is unexpected due to the higher contribution from secondary electrons in the simulation, as described above. The NCRP-40 data is thus found to over predict the dose from an encapsulated source, based on a combination of overstating the photon component and understating the secondary electron emission compared to the simulation data. The overstatement of the dose rate is only applicable to the exact source models described in NCRP-40. It is seen in publications cited in this research (Saenger, Kereiakes, Wald, & Thoma, 1974) that the practical use of the secondary electron correction factors involves measurement of the gamma emission for the source type in an exposure scenario and applying the dose correction factor to that data. Therefore, the critical parameter is the secondary electron correction factor, as the photon emission will be detected case by case. The simulation data shows a larger secondary electron correction factor, which if applied as a dose conversion factor to a photon measurement would assign a higher dose than the same factor proposed by NCRP-40.

Evaluation of the difference seen in the photon dose rates described above is not in the scope of the current research. Recommendations regarding the discrepancy are made in Chapter 5.

The correction factor for simulation data converges to that stated in NCRP-40 as the distance from the source surface increases. The correction factor at the furthest boundary evaluated, at 0.1 cm depth in tissue, the factors stated each are approximately equal, at 45%, (Table 7). This indicates that the correction factor stated in NCRP-40 is not only far below the actual condition seen at the source surface, but would only apply to a region in excess of the range of the secondary electron from the encapsulated source (Section 4.1).

The above results show significant differences in the secondary electron corrections factors, which are determined by relative comparison of the photon only dose rate, with the absolute value of the secondary electron emission. This non-conformance is attributable to the historical studies that are cited by NCRP-40 to obtain the data for the correction factors. Those studies have been shown to lack the required sensitivity to evaluate the very near surface emission conditions for an encapsulated gamma source (Section 4.2 and 4.3).

The evaluation of dose at increasing depth in tissue (Table 7) does not apply to the surface dose rate values from NCRP-40. However there is a comparable basis to other studies which examined the decreasing contribution of secondary electrons generated from the capsule wall with increasing distance in tissue, measured at increasing intervals from the source surface (Tripathi, 1977). The intention of those studies was to quantify the region of tissue that should be considered when attributing dose from secondary electron radiation. A dose conversion factor expanded to a region beyond the surface is valuable for assigning dose once an insult has been received. The surface dose conversion factor will describe the region of highest deposition, and is useful for radiation protection requirements. A dose conversion factor applicable to the layer of tissue that is affected by secondary electron emission will

more accurately describe the actual dose committed to the tissue layer affected. This factor for the region 0 cm to 0.1 cm is described in Section 4.4.

4.3.3 Results and Analysis - Additional Nuclides

Total dose rates and correction factors for secondary electron emission were published for Co-60, Cs-137 and Ir-192 in NCRP-40 (1972) for the same encapsulated source model as the Ra-226 described Chapter 3. These sources were also simulated, and measurements recorded for the photon only and total dose rates, and resultant secondary electron dose correction factor calculated. The correction factors are as follows: Co-60 at 620%, Cs-137 at 290% and Ir-192 at 207%. For these source models NRCP recommends a correction factor of 25-45%, which is a difference of 3.6 – 13.7 times the values found by simulation (Table 10). The rational for this discrepancy is described in Section 4.3.2.

4.4 Surface Dose Rate, External Application

The work by Tripathi (1977) examines the dose rate to the hands of medical technologists handling Tc-99m liquid source, encased in a plastic syringe. The focus of that research is a determination of the dose rate from an encapsulated gamma ray source from an external point of reference. This is achieved by assessing the energy deposition in the living tissue layers under the epidermal layer, depth from 0.01-0.1 cm. This study used a numerical Monte Carlo software model to simulate the secondary dose rate at increasing intervals of distance from the source, to show the decreasing significance of secondary electron contribution to the dose with increasing distance. Tripathi also made a recommendation for a total dose rate for the living tissue layer under the epidermal layer, at 0.02 cm depth.

This study is not directly comparable to the data in NCRP-40 as the source models differ, however the trend (Figure 7) for dose rate at depth in tissue corresponds to that seen for the simulation of the NCRP-40 source model with increasing depth (Figure 15 and 16), demonstrating that the simulation is consistent with the expected decrease of secondary electron radiation with distance from the source.

In the replication of the Tripathi study, the Radium-226 source model from the NCRP-40 simulation was used, and three trials were executed with a varying depth tissue layer detector designated based on the recommendations in Tripathi. The detector layer for each trails are: 0-0.01 cm, 0.01-0.1 cm, and 0-0.1 cm at a depth in tissue located radially from the source surface. These regions correspond to: the region of highest dose at the surface, the region of active tissue in the sub-dermal layer (for external dose applications), and the total travelled path length of the secondary electron radiation. For all cases the correction factor is presented to demonstrate the relative proportion of the secondary electron emission in the external application scenario.

The result from this simulation will provide the secondary electron correction factor and dose conversion factor for the regions of interest where interactions from secondary electron predominantly occur, for both internal and external exposure scenarios.

4.4.1 Results

The data from the Tripathi study is shown in Figure 7. The simulation results from MCNPX are shown in Table 11. The simulation data in this research is not directly comparable to that from Tripathi as the source models are different. The recommendations in Section 4.4 are based on the format from NCRP- 40 for secondary electron correction factors and dose conversion factors for encapsulated sources of Radium-226, applicable to the regions of interest defined by Tripathi.

Table 11: Dose Rate at in Tissue Layer, External and Internal Scenario –Simulation Data, NCRP Source Model

Region	Target Depth (cm)	Photon Only Dose (R/min-Ci)	Photon Only FSD	Total Dose (R/min-Ci)	Total FSD	Secondary Electron Correction Factor (%)
1	0 - 0.01	6.58E-05	6.8E-03	2.74E-04	6.1E-03	316
2	0.01 - 0.09	1.10E-03	7.0E-03	1.76E-03	6.3E-03	60
3	0 - 0.1	1.15E-03	7.1E-03	1.97E-03	6.1E-03	72

Region 1, near surface 0-0.01 cm, shows a relative intensity of secondary electron of 4.16, corresponding to a correction factor for secondary electrons of 316%. This result is consistent with the simulation results in Section 4.2 and 4.3, for surface dose rates of the NCRP-40 and Benner models. Good agreement is expected as the 0.01 cm depth detector is similar to the 0.007 depth used in the previous simulations. This correction factor is applicable as part of the dose conversion factor for exposure at the source surface.

Region 2, near surface 0.01-0.09 cm, shows a secondary electron correction factor of 60%. This target range is the region of interest in a dose attribution scenario for external exposures seen in the work by Tripathi. This correction factor is applicable to any scenario for an external exposure where the dose rate in the active tissue layer is of interest. Region 3, near surface 0-0.1 cm, shows a secondary correction factor ratio of 1.72, a correction factor of 72%. This represents the contribution due to secondary electrons for the total travelled path length of the secondary electrons, and is applicable to an evaluation

of an internal exposure, where the entire range of secondary electrons from the source surface requires evaluation.

4.4.2 Analysis

The secondary electron correction factors for Regions 2 and 3, of 60 and 72%, are in close agreement with the NCRP-40 value for the surface emission 45%, where those regions examined energy deposition over the total travelled path of the secondary electron emission. In Section 4.2 and 4.3 of this thesis it is shown that the 45% correction factor from NCRP-40 is derived from the physical trials performed by Benner, where those trials lacked the required sensitivity to evaluate the emission condition at the very near surface of the source The experimental results from Benner (1931) were also shown to apply over the approximate total range of the secondary electrons (Section 4.3). Therefore, this agreement (above) is expected.

Closer agreement with the Benner (1931) data is observed if an additional factor is considered regarding the reporting of the secondary electron correction factors recommended by Benner (Section 2.3). In the case of the Iron encapsulated source model, which is the data referenced by NCRP-40 for secondary electron correction factor, Benner (1931) proposes a 59-63% value. In the summary of the Benner (1931) work by Attix (1969), a 45% correction factor is recommended citing the Benner (1931) experiment. It is uncertain at the time of this current study why the discrepancy exists. The 45% value appears in the Benner (1931) study as an uncorrected data point, and it may have been selected for reference unknowingly. Regardless of the cause, if the correction factor of 59-63% is used, as recommended by Benner (1931) then the simulation data for Region 2 and 3 of 60-72%, as described above is in very good agreement with the historical study.

CHAPTER 5 CONCLUSIONS and RECOMMENDATIONS

This research was undertaken to improve the semi-analytical contact dose conversion factors found in in NCRP Report No. 40. As such, this research involves bounding the radiation hazard at the surface of encapsulated gamma ray sources, and several discrete results that deviated significantly from the published values were found. Three distinct simulation results predominate: the secondary electron component is underestimated at high atomic number encapsulation materials, the secondary electron component is understated in recommended correction factors, and the emission measured over the maximum range of the secondary electron emission in tissue showed good agreement with secondary electron correction factors and relative intensities seen in NCRP–40.

The first notable result is observed for the simulations executed replicating the Benner source, where the both the total emission and the component of secondary electron radiation was measured as a function of capsule material. The simulation shows data that exceeds all of the absolute values of Benner, but conforms to the relative gradient for differences between data points up to atomic number 58, as seen in Figure 13. At those highest value atomic number material the results from the simulation show values far in excess of Benner, and also in excess the relative trend (Figure 13). Application of the data from the research by Benner (1931), will underestimate the secondary electron hazard at all encapsulated sources studied, with the most egregious difference at the higher atomic number encapsulations. Incorrect recommendations for the level of hazard represented by that type of source configuration would result from referencing the data, leading to unanalyzed exposures levels.

The second prominent result was observed from the data obtained in the simulation of the NCRP-40 source models, which was conducted to reanalyze the secondary electron correction factors for the source

model stated in NCRP-40. The correction factors obtained in the simulation exceed those proposed by NCRP-40 by a factor of 8. This result indicates that for a measured gamma dose rate for an encapsulated Ra-226 source, if corrected by the secondary electron factor from NCRP-40, it will be understated by a factor of 8. This type of event would lead to ineffectual early medical treatment of exposures and incorrect correlation of dose to tissue damage. Additionally, radiation protection practices would be inaccurate, as the contact hazard is not well described. The combined effect worsens the diagnosis and medical treatment of radiation injuries from contact with and encapsulated gamma source. Future work should update the secondary electron correction factors stated in NCRP-40, and perform additional simulations for other commonly used source configurations, supplying secondary electron correction factors which correctly account the actual emission.

The third result of distinction is observed in the simulation data for the ranges in tissue around an encapsulated source of 0-0.1 cm for internal exposures and from 0.01-0.1 cm for external cases.

The secondary electron correction factor for the internal case is found to be 72% which is in close agreement with that recommended by NCRP-40 of 45% and that stated in Benner of 59-63%. The detection of simulated radiation interactions through 0.1 cm tissue depth is representative of the average energy deposition, where higher dose rates are seen at the source surface and decline exponentially as the distance from the source increases (Figure 15 and 16). The 72% dose conversion factor is only useful for those cases where an insult has occurred and the absorbed dose to a tissue *layer* is required to be determined. This factor should not be applied for radiation protection purposes as it does not accurately describe the region of the highest dose, which is at the source surface. Similarly for the case of external exposure, the secondary electron correction factor is 60%, where the restrictions described above are equally applicable.

Future work should include physical experiments performed to confirm the simulated results observed in this thesis , with focus on the proportion of secondary electron emission at the source surface, and the increasing intensity of this type of radiation generated in materials of an atomic number higher than 60. For external and internal exposure scenarios, additional physical experiments and/or simulations should be conducted to confirm the secondary electron correction factor found for those regions of interest within the range of secondary electrons. This type of correction factor should be published in addition to those for surface conditions, such that a dose may be assigned to the entire effected tissue layer post injury. Accurate contact dose rate data for encapsulated sources will aid medical treatment and retrospective dosimetry in cases of accidental exposure, and enable the selection of appropriate shielding materials to maximize radiation protection.

REFERENCES

Los Alamos National Laboratory. (2007). Monte Carlo N Particle (MCNPX), Version 2.6.0. Los Alamos, Naw Mexico, United States of America.

Baratta, A. J., & Lamarsh, J. R. (2001). *Intorduction to Nuclear Engineering .* Prentice Hall Inc.

Benner, S. (1931). On Secondary β-Rays from the Surface of Radium Containers. *Acta Radiologica [Old Series]*, 401-412.

LANL. (2005). *MCNPX User's Manual.* Los Alamos: Los Alamos National Laboratory.

National Council on Radition Protection and Measurments. (1972). *Protection Against Radiation from Brachytherapy Sources.* Washington D.C.: NCRP.

NCRP. (1972). *NCRP Report No. 40*.

NCRP. (1972). *Protection Against Radiation from Brachytherapy Sources.* Washington D.C.: NCRP, Protection Against Radiation from Brachytherapy Sources.

Quimby, E. H., Marinelli, L. D., & Blady, J. V. (1939). *Secondary Filters in Radium Therapy.* San Francisco: American Radium Society.

Saenger, E., Kereiakes, J., Wald, N., & Thoma, G. (1974). *Clinical Course and Dosimetry of Acute Hand Injuries to Industrial Radiographers from Multicurie Sealed Gamma Sources.* Cincinnati: University of Cincinnati.

Shalek, R. J., Stoval, M., Attix, F., & Tochilin, E. (1969). Dosimetry in Implant Therapy. *Radiation Dosimetry, Vol 3, Sources, Fields, Measurements and Applications*, 743.

Team, X.-5. M. (2003). *MCNP – A General N-Particle Transport Code, Version 5.* Los Alamos: Los Alamos National Laboratory.

Tripathi, A. (1977). *Determination of Skin Dose to the Hands of Technologists Handelling Syringes Containing Radiopharmaceuticals.* Corvallis: Radiation Center, Oregon State University.

Waller, E. (Winter 2011). Introductory MCNP, using MCNP4a. *Monte Carlo Methods*.

Wilson, C. (1941). *The Dependence of the Secondary Electronic Emission Produced by Gamma Radiation Upon the Direction of the Radiation.* London: Physics Department, Westminster Hospital.

APPENDIX A: MCNPX CODES WRITTEN FOR THESIS

Total surface dose rate – NCRP-40 Source Model

```
Ra-226 encapsulated source, electron energy deposition
c
c      This code will calculate the Total absorbed dose to a 0.007cm
c      cylindrical target layer (H20) at 0.1cm from the surface of the
c      source through tissue. Encapsulation of Stainless steel (304);
c      This is the source model described in NCRP-40
c
c
c
c      Cell Cards
    1     0          -1       $ Ra-226 source material (made void)
   10   265       -8 -10 1    $ Wall material
   15   280       -1 -15 10   $ Target
   17   280       -1 -17 15   $ Target2
   20   280       -1 -20 17   $ Backing tissue layer
   30     0          -999 20  $ Void
  333     0          999      $ External void

c      Surface Cards
    1       rcc -0.5 0 0 1 0 0 0.2375         $Cs source cylinder
   10       rcc -0.58 0 0 1.16 0 0 0.3175     $Wall (0.08cm)
   15       rcc -0.59 0 0 1.18 0 0 0.4175     $Target 1 (0.1cm)
   17       rcc -0.6 0 0 1.2 0 0 0.4245       $Target 2 (.007cm)
   20       rcc -1.2 0 0 2.2 0 0 1.4245       $Backing (1.0cm)
  999        so 10                            $outer void

mode  p e
c
c
c      Material Cards
c
c
c           Air
m204  7000.          -0.755636  $MAT204
      8000.          -0.231475 18000.        -0.012889
c
c           Water
m280  1000.          -0.111915  $MAT280
      8000.          -0.888085
c
c           Source
m301  88226.04p          0.166  $MAT301
      8000.              0.668 16000.            0.166
c
c           Wall (SS-304)
m265  6000.02p         -0.0003  $MAT265
```

```
      14000.02p        -0.005 15000.02p     -0.000225 16000.02p      -
0.00015
      24000.02p         -0.19 25000.02p         -0.01 26000.02p     -
0.701825
      28000.02p       -0.0925
c
c
c      Transport Importance per Cell
c
c
imp:e   1 5r         0             $ 1, 333
imp:p   1 5r         0             $ 1, 333
c
c
c      Source Cards
c
sc1   Ra-226 pure gamma source (from progeny Bi-214 and Pb-214)
sdef  PAR=2 erg=d1 pos=-0.5 0.0 0.0 rad=d2 ext=d3 axs=1 0 0
#     si1    sp1
      0      0
      0.18   0.012
      0.241  0.115
      0.294  0.258
      0.350  0.450
      0.607  0.658
      0.766  0.065
      0.933  0.067
      1.120  0.206
      1.238  0.063
      1.379  0.064
      1.761  0.258
      2.198  0.074
si2  0 0.2375
sp2 -21 1
si3  0 1
sp3 -21 0
c
c
c      Tally Cards
c
c
fc16   Electron (i.e. total) energy deposited over cell 15 (avg)
f16:e 15
sd16  1     $unity on this card converts tally to MeV
e16    0.05 0.1 0.15 0.2 0.25 0.3 0.35 0.4 0.45 0.5 0.55 0.6 0.65 0.7
       1.0 1.5 2.0 2.5
c
fc26   Electron (i.e. total) energy deposited over cell 17 (avg)
f26:e 17
sd26  1     $unity on this card converts tally to MeV
e26    0.05 0.1 0.15 0.2 0.25 0.3 0.35 0.4 0.45 0.5 0.55 0.6 0.65 0.7
       1.0 1.5 2.0 2.5
c
c      Physics cards
```

```
phys:p 2.198
cut:p  1j 1E-3
phys:e 2.198
dbcn   17j 1       $Use ITS electron algorithm
c
c
c      History Cutoff
c
c
nps    2000000
print
prdmp 2000000 2000000 1



imp:e   1            0            1 3r         0             $ 1, 333
imp:p   1 5r         0             $ 1, 333
```

Photon only surface dose rate – NCRP-40 Source Model (all secondary electrons blocked in wall region)

```
Ra-226 encapsulated source, electron energy deposition
c
c      This code will calculate the Total absorbed dose to a 0.007cm
c      cylindrical target layer (H20) at 0.1cm from the surface of the
c      source through tissue. Encapsulation of Stainless steel (304);
c      This is the source model described in NCRP-40
c
c
c
c      Cell Cards
    1     0          -1       $ Ra-226 source material (made void)
   10   265       -8 -10 1    $ Wall material
   15   280       -1 -15 10   $ Target
   17   280       -1 -17 15   $ Target2
   20   280       -1 -20 17   $ Backing tissue layer
   30     0          -999 20  $ Void
  333     0          999      $ External void

c      Surface Cards
    1       rcc -0.5 0 0 1 0 0 0.2375         $Cs source cylinder
   10       rcc -0.58 0 0 1.16 0 0 0.3175     $Wall (0.08cm)
   15       rcc -0.59 0 0 1.18 0 0 0.4175     $Target 1 (0.1cm)
   17       rcc -0.6 0 0 1.2 0 0 0.4245       $Target 2 (.007cm)
   20       rcc -1.2 0 0 2.2 0 0 1.4245       $Backing (1.0cm)
  999        so 10                            $outer void

mode  p e
c
c
c      Material Cards
c
c
c           Air
m204  7000.          -0.755636  $MAT204
      8000.          -0.231475 18000.        -0.012889
c
c           Water
m280  1000.          -0.111915  $MAT280
      8000.          -0.888085
c
c           Source
m301  88226.04p         0.166  $MAT301
      8000.              0.668 16000.            0.166
c
c           Wall (SS-304)
m265  6000.02p        -0.0003  $MAT265
      14000.02p        -0.005 15000.02p     -0.000225 16000.02p      -
0.00015
```

```
      24000.02p         -0.19 25000.02p         -0.01 26000.02p     -
0.701825
      28000.02p       -0.0925
c
c
c      Transport Importance per Cell –
c      *This is where the secondary electrons are filtered (blocked) by
c      setting the wall region to zero importance*
c
c
imp:e   1            0            1 3r         0             $ 1, 333
imp:p   1 5r         0             $ 1, 333
c
c
c      Source Cards
c
sc1   Ra-226 pure gamma source (from progeny Bi-214 and Pb-214)
sdef  PAR=2 erg=d1 pos=-0.5 0.0 0.0 rad=d2 ext=d3 axs=1 0 0
#     si1    sp1
      0      0
      0.18   0.012
      0.241  0.115
      0.294  0.258
      0.350  0.450
      0.607  0.658
      0.766  0.065
      0.933  0.067
      1.120  0.206
      1.238  0.063
      1.379  0.064
      1.761  0.258
      2.198  0.074
si2  0 0.2375
sp2 -21 1
si3  0 1
sp3 -21 0
c
c
c      Tally Cards
c
c
fc16   Electron (i.e. total) energy deposited over cell 15 (avg)
f16:e 15
sd16  1     $unity on this card converts tally to MeV
e16    0.05 0.1 0.15 0.2 0.25 0.3 0.35 0.4 0.45 0.5 0.55 0.6 0.65 0.7
       1.0 1.5 2.0 2.5
c
fc26   Electron (i.e. total) energy deposited over cell 17 (avg)
f26:e 17
sd26  1     $unity on this card converts tally to MeV
e26    0.05 0.1 0.15 0.2 0.25 0.3 0.35 0.4 0.45 0.5 0.55 0.6 0.65 0.7
       1.0 1.5 2.0 2.5
c
c
```

```
c     Physics cards
c
phys:p 2.198
cut:p  1j 1E-3
phys:e 2.198
dbcn   17j 1       $Use ITS electron algorithm
c
c
c      History Cutoff
c
c
nps    2000000
print
prdmp 2000000 2000000 1
```